Approved for public release;
distribution unlimited.

AD-A277 274

CUMENTATION PAGE

Form Approved
OMB No. 0704-0188

2. REPORT DATE	3. REPORT TYPE AND DATES COVERED
17 January 1994	Final April 1, 1990 - November 30, 1993

4. TITLE AND SUBTITLE

Pressureless Sintering of Ceramic Composites

5. FUNDING NUMBERS

AFOSR-90-0265
UNM 320581

(2)

G/ISD
3484/KD

6. AUTHOR(S)

Martin William Weiser

DTIC
ELECTE
MAR 23 1994
S F D

7. PERFORMING ORGANIZATION NAME(S) AND ADDRESS(ES)

Mechanical Engineering Department and
Center for Micro-Engineered Ceramics
University of New Mexico
Albuquerque, NM 87131-1361

8. PERFORMING ORGANIZATION REPORT NUMBER

AFOSR-TR- 94 0056

9. SPONSORING / MONITORING AGENCY NAME(S) AND ADDRESS(ES)

Alexander Pechenik
Air Force Office of Scientific Research
Electronic and Materials Science Program
Bolling Air Force Base, DC 20332-6448

10. SPONSORING / MONITORING AGENCY REPORT NUMBER

AFOSR-90-0265

11. SUPPLEMENTARY NOTES

None

94-09050

12a. DISTRIBUTION / AVAILABILITY STATEMENT

No limitations

Approved for public release;
distribution unlimited.

13. ABSTRACT *(Maximum 200 words)*

This project examined the pressureless sintering and densification behavior of model ceramic composites. The effect of inclusion aspect ratio on densification was studied using SiC whiskers and fibers in an Al_2O_3 matrix. Composites had maximum sintered density when made from fibers with aspect ratios around ten. This peak in the density is a result of the density of short aspect composites being inhibited by inclusion size considerations while long aspect composites are prevented from densifying by percolation related effects. How inhomogeneous inclusion distribution affects densification was studied using SiC_p/Al_2O_3 composites. Three different types of inhomogeneity known as concentration, amplitude, and size were investigated. The sintered density was maximized at moderate levels of inclusion inhomogeneity. We also found that various salts were effective coagulating agents for slip casting Al_2O_3/ZrO_2 composites. The drying of composites found that percolation limits the green density of particulate composites. The fracture toughness of Mn-Zn ferrites was increased from 0.9 MPa$\sqrt{m}$ to 2.8 MPa$\sqrt{m}$ by addition of 25 vol% partially stabilized ZrO_2. Transient liquid phase sintering of composites is not an effective densification method.

14. SUBJECT TERMS

Ceramic Composites, Sintering, Densification, Inclusion Distribution, Inclusion Aspect Ratio, Drying, Toughening, Ferrites, Slip Coagulation

15. NUMBER OF PAGES

63

16. PRICE CODE

17. SECURITY CLASSIFICATION OF REPORT	18. SECURITY CLASSIFICATION OF THIS PAGE	19. SECURITY CLASSIFICATION OF ABSTRACT	20. LIMITATION OF ABSTRACT
Unclassified	Unclassified	Unclassified	

NSN 7540-01-280-5500

Standard Form 298 (Rev. 2-89)
Prescribed by ANSI Std. 239-18

94 3 22 054

Pressureless Sintering of Ceramic Composites

Martin W. Weiser
Mechanical Engineering Department and
UNM/NSF Center for Micro-Engineered Ceramics
University of New Mexico
Albuquerque, NM 87131

Final Report
April 1, 1990 - November 30, 1993 Work Period
April 1, 1990 - March 31, 1993 Funding Period
$146,424 Total Funding

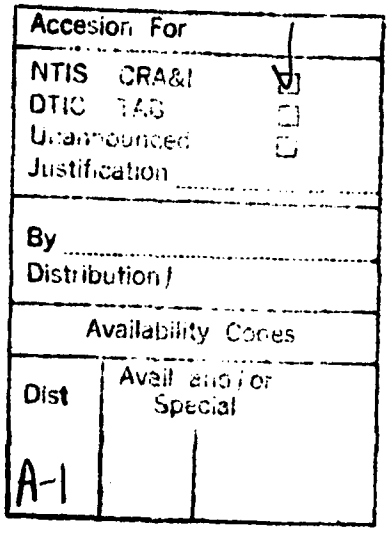

1 Project Overview

This project was initiated to examine the pressureless sintering and densification behavior of two different types of model ceramic composites. The first studied the effect of inclusion aspect ratio on densification while the second examined how inhomogeneous inclusion distribution affects densification. The scope of the project was expanded to include three closely related activities in ceramic processing: drying of composites, fabrication of toughened ferrites, and transient liquid phase sintering of composites.

The effect of inclusion aspect ratio study investigated the use of both SiC whiskers (≈ 0.4 μm diameter) and fibers (≈ 15 μm diameter) in a fine grained Al_2O_3 matrix (≈ 0.39 μm diameter). Both whiskers and fibers were difficult to fractionate into distributions with distinct aspect ratios. Only two distributions were obtained for the whiskers while six distributions were obtained for the fibers. Composites containing 0.00 to 0.34 volume fraction of these fiber distributions were made by slip casting and fired at 1400°C for four hours. The green density was independent of the fiber aspect ratio but depended strongly on the volume fraction. The sintered density depended on both the volume fraction and aspect ratio. A peak in the sintered densities of composites made with less than 0.15 volume fraction of fibers was found at aspect ratios of 8 to 12. The sintered density of composites containing higher volume fractions decreased monotonically with increasing aspect ratio. The peak in the density is a result of the density of short aspect composites being inhibited by inclusion size considerations while long aspect composites are prevented from densifying by percolation related effects. However, we did not see classic percolation behavior in which the density drops dramatically with increasing volume fraction or aspect ratio. This is a result of high quality green processing which prevents the formation of a rigid percolation network.

The densification of inhomogeneous composites was studied using 4 μm SiC particles in a 0.68 μm Al_2O_3 matrix. Three different types of inhomogeneity known as concentration, amplitude, and size were investigated. The sintered density was maximized at moderate levels of inclusion inhomogeneity. We initiated, but did not complete, a study of similar Al_2O_3/ZrO_2 composites since other investigators have shown that moderate levels of inhomogeneity in these materials result in improved fracture toughness. The study of Al_2O_3/ZrO_2 composites ended with an investigation of the effect of coagulating salt on the green and sintered density of homogeneous composites that were to be the precursors for the study of inhomogeneity. We found that several different salts can be used to coagulate the slips successfully. Aluminum based salts are potentially very useful once problems with the suspension pH are corrected.

Three small supplemental studies of related topics were conducted with the assistance of four undergraduate students, three of which were from underrepresented minority groups. The drying of composites found that percolation limits the green density of particulate composites. The percolation limit is higher than predicted based upon the inclusion morphology due to the capillary forces generated during drying. The fracture toughness of Mn-Zn ferrites was increased from 0.9 MPa$\sqrt{m}$ to 2.8 MPa$\sqrt{m}$ by addition of 25 vol% partially stabilized ZrO_2. This addition decreased the magnetic permeability of the materials, but it is felt that optimization of the microstructure would allow reasonable values of the permeability. Transient liquid phase sintering of composites is not an effective densification method since the liquid is not present long enough for the rearrangement of the inclusions necessary for densification.

This project has improved our understanding of ceramic processing and described several approaches that may allow low cost fabrication of high quality ceramic matrix composites via pressureless sintering. The project did not achieve all of its goals since these were too ambitious for the resources requested and available. However, there have been several presentations in the area, one publication is in print, and several others are being prepared. In addition, this project has contributed significantly to the education of several students including several members of underrepresented minority groups.

2 Inclusion Aspect Ratio

2.1 SiC Whiskers

2.1.1 Whisker Fractionation

The first year of this study was devoted to developing a technique for fractionating small quantities of fine (0.2-0.5 μm diameter) SiC whiskers (American Matrix) of different lengths. This proved to be a rather difficult endeavor but a usable, although not total satisfactory, technique was developed. The as received whiskers are ground using SiC media in a vibratory mill for 0.5 to 72 hours. The shorter grind times are intended to simply break up the agglomerates while the longer grinding times are designed to break the whiskers into shorter sections. The whiskers are then dispersed using polyethyleneimine (PEI) and sedimented in a 500 ml buret to improve the uniformity of the length distribution. This process yielded two different volume fractions of SiC_w with average lengths of 2.4 and 18.7 μm and a wider distribution than desired. This yields average aspect ratios of approximately 6 and 45 based upon the average whisker diameter of $\approx$0.4 μm.

Vibratory milling was found to introduce foreign particles into the SiC_w solution from the SiC balls used as the grinding media. The foreign particles' possible effect on the results was undesirable so this method was discontinued. The next method of separation consisted of sedimentation of the as received whiskers using a 1 l buret, polyethyleneimine dispersant, glycerin, and water. This method produced two different distributions with lengths of 5.89$\pm$6.20 μm for the decantant and 13.07$\pm$10.71 μm for the sediment as shown in Figure 1. Unfortunately, the distribution of both fractions is much too wide to yield high quality information on the aspect ratio effects. However, Al_2O_3/SiC_w composites were fabricated using these whiskers as discussed later.

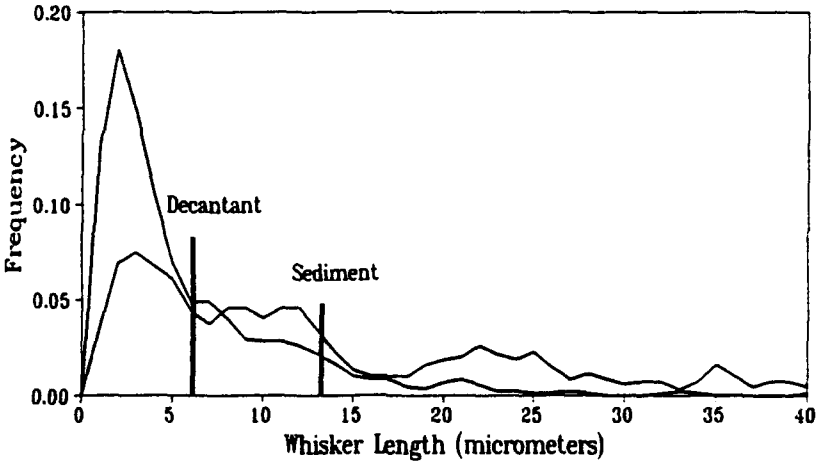

Figure 1 Distribution of the SiC_w lengths for the as received whiskers that had been sedimented for 12 hours. The vertical lines mark the average lengths for each distribution.

The next step was the use of a hydrocyclone to classify the whiskers. This yielded preliminary results that are more promising than the other separation methods. A hydrocyclone is a conically shaped piece of equipment that uses a fluid flow to create a rotational fluid motion. The rotational motion of the fluid produces centrifugal forces on the SiC whiskers suspended in the fluid which forces separation of the different size whiskers. Fluid rotation is caused by injection of the fluid into the feed inlet of the hydrocyclone shown in Figure 2. The fluid spirals down the conical section of the apparatus. As the fluid reaches the underflow outlet some of it flows out. However, most of it cannot because the underflow outlet is designed to restrict flow. The remaining fluid flows toward the center of the hydrocyclone and rises to the overflow outlet. Separation occurs because the longer, heavier whiskers are flung to the sides of the cyclone and ultimately flow down and out the underflow outlet. Smaller, lighter whiskers are forced to the center of the cyclone and then up and out the overflow outlet. The process can be repeated on the overflow and underflow whiskers to separate each of those into different sized whiskers.

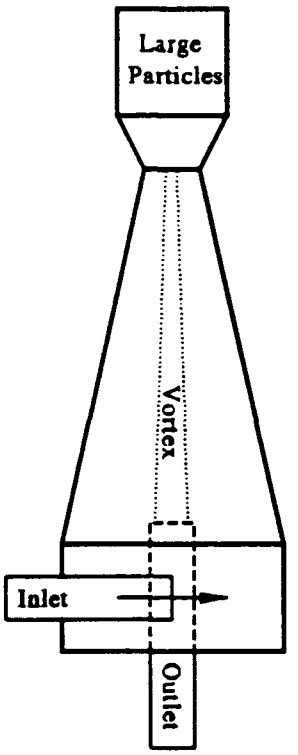

Figure 2 Principle features of a hydrocyclone. From The Hydrocyclone by D. Bradley[1].

The hydrocyclone was not as effective in separating the whiskers by length as was hoped. Typical distributions are shown in Figure 3 where it is seen that the distributions are quite wide and are multimodal. Three different distributions were obtained with average lengths of 6.9, 11.8, and 17.3 μm. However, the distributions overlapped too much to be useful.

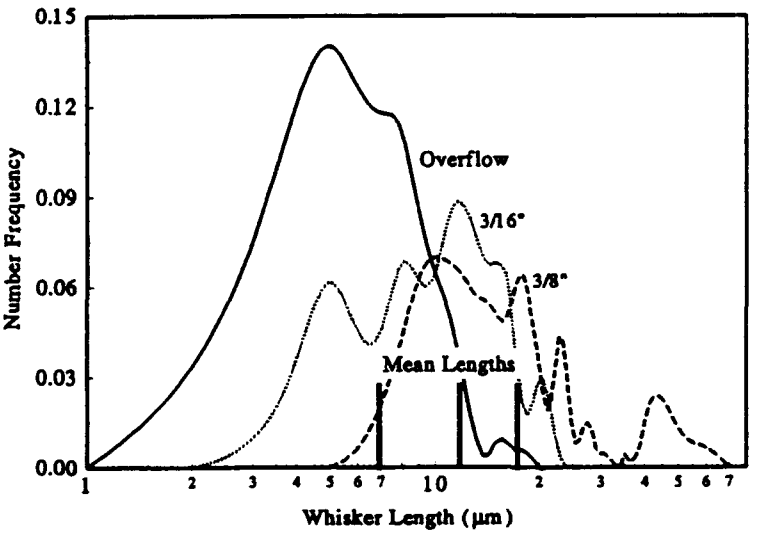

Figure 3 SiC whisker distributions from the hydrocyclone.

At this point we decided that fractionation of the whiskers was not feasible given the available resources. Therefore, we turned to fractionation of SiC fibers that were approximately 15 μm in diameter as discussed in section 2.2. Some fibers were separated using the inverted hydrocyclone, but the results were similar to those obtained using the whiskers. Therefore, other techniques were used to fractionate the fibers as described in section 2.2.1.

2.1.2 Densification of SiC_w Composites

The two whisker fractions shown in Figure 1 were used to fabricate composites for a preliminary study of the densification behavior. Composite pellets containing volume fractions of 0.00, 0.025, 0.05, and 0.10 of the two SiC_w distributions in a Sumitomo AKP-50 Al_2O_3 matrix were slip cast under either acidic (pH=4.5) or alkaline (pH=10.5) conditions and sintered at 1400°C. Figure 4 shows that the addition of the whiskers impeded the densification significantly when the slips were fabricated under acidic conditions but there was only a small effect under alkaline conditions.

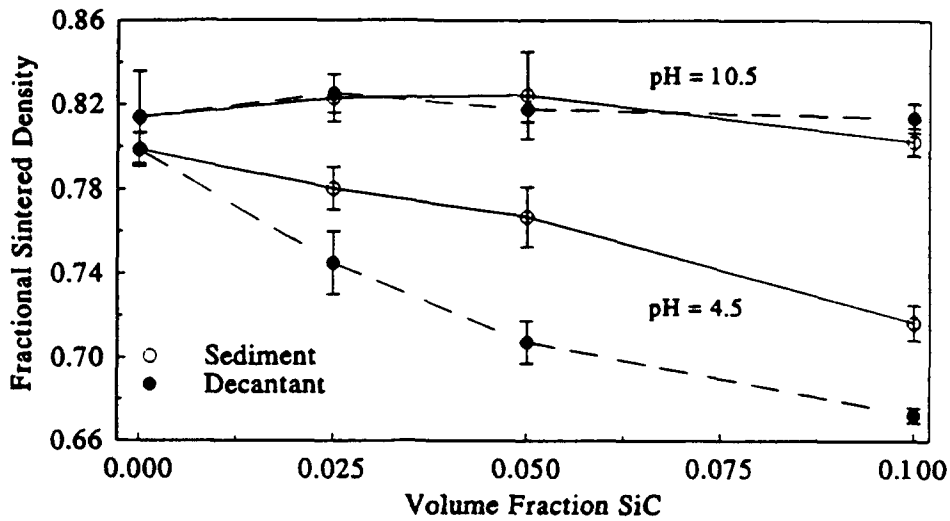

Figure 4 Fractional sintered density of the composites made with the sedimented SiC_w and AKP-50 Al_2O_3 after firing at 1400°C for 4 hrs. The pH of the slip is given.

These effects can be explained by considering the effects of green processing as shown in Figure 5. The addition of whiskers to the composites made under acidic conditions did not affect the fractional green density which was quite low with values between 0.45 and 0.50. On the other hand, the addition of whiskers enhanced the green density of the composites made under alkaline conditions. The net result is that the impediment of densification is fully seen upon sintering the composites made with an acidic slip while a large portion of the impediment is masked by the increased green density with the addition of whiskers for the alkaline slips. The details of this interaction between the green processing and the final density of the composites were not pursued at this time since we had decided that the distribution of the SiC_w fractions were not narrow enough using this separation technique.

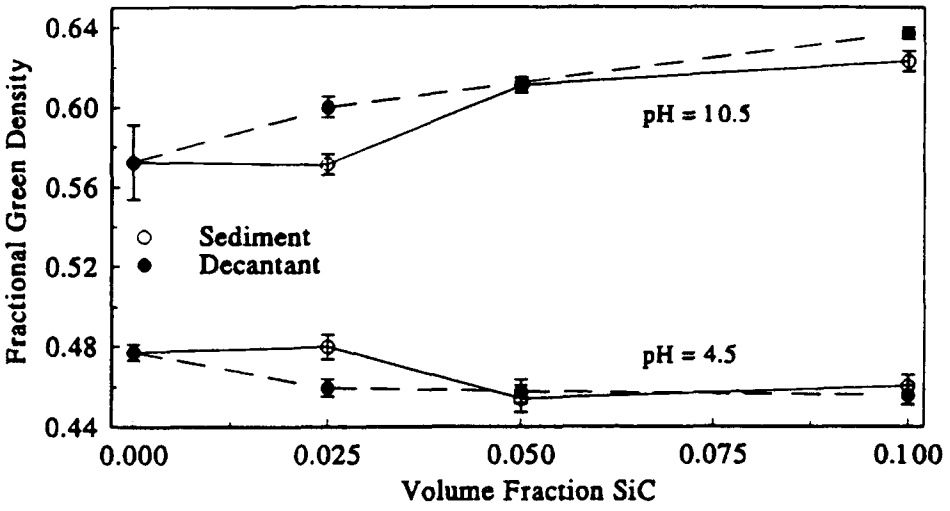

Figure 5 Fractional green density of the slip cast pellets made from the sedimented SiC_w and AKP-50 Al_2O_3. The pH of the slip is given.

2.2 SiC Fibers

The most difficult portion of this study was separating the SiC fibers into different aspect ratios. Whiskers were initially investigated for use in this study as discussed above. However, it was not possible to create several narrow aspect ratio distributions from the whiskers because of their small size (0.4 μm diameter). Larger SiC fibers ($\approx$ 15 μm diameter) were then chosen, and successfully separated into six different distributions using a combination of ball milling, sedimentation, and sieving. These fibers were then incorporated into Al_2O_3/SiC_w composites via slip casting. The green density, sintered density, and microstructure of these composites were analyzed.

2.2.1 Fiber Fractionation

Fractionation of the Five Highest Aspect Ratios

The Nicalon™ Silicon Carbide fibers (Dow Corning, Midland, Michigan) were M sized and received as chopped 600 denier yarn 1 mm in length. They were heated to 600°C in air for 0.5 hours to burn off the adhesive keeping the individual fibers in denier form. After the heat treatment a density 2.6565 $\pm$ 0.0121 g/cm^3 was measured using helium pycnometry. The average fiber diameter was 15.32 $\pm$ 1.61 μm via SEM examination. Nicalon SiC fibers have been analyzed by other investigators and have an approximate composition of 50% SiC, 39% carbon, and 11% SiO_2[2].

The five longest distributions were produced by vibratory milling 5 grams of the fibers in a 250 ml Nalgene container along with 300 grams of 6.7 mm diameter SiC ball media and

deionized water for 30 minutes. This produced large numbers of submicrometer chips from collision of the SiC ball media with itself and with the fibers.

Sedimentation of the aqueous SiC suspension in a 1 l buret removed most of the small particles. One liter of suspension was sedimented for one hour in the buret and 100 ml of sediment was drawn off while the decant was discarded. The sediment was redistributed with 900 ml of fresh water and resedimented a total of five times. This produced approximately 2.5 grams of relatively chip free fibers ranging from < 1 to 400 μm in length. The fibers were separated into six different aspect ratio distributions via a specialized sieving process followed additional sedimentation for the two lowest aspect ratios.

Figure 6 shows the sieving apparatus while Table I describes the stainless steel sieves used to separate the SiC fibers. The sieving procedure was to add the 2.5 g of vibratory milled fibers to 250 ml of deionized water, and then to pour the mixture into a 1 l buret. Opening the stopcock allowed the suspension flow onto a plastic which bent the stream so that the suspension flowed off the sheet nearly parallel to the top surface of the sieve screen. The edge of the plastic was beveled to give a smooth transition from the plastic sheet to the wire mesh. Separation occurs because long fibers will span one or more openings in the sieve while short ones will fall through. Our analysis of the criteria for fiber separation is discussed after the results of the process are presented.

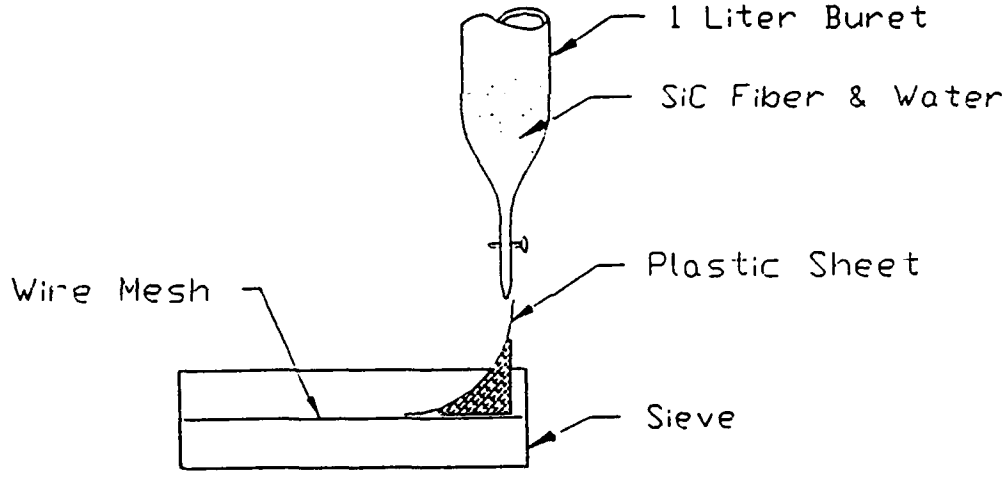

Figure 6 Equipment setup for the sieving process.

Table I Sieve opening sizes, standard deviations, and maximum size of opening.

Average Sieve Opening (μm)	Wire Diam. (μm)	Permissible Opening Deviation (μm)	Maximum Individual Opening (μm)
90	64	$\pm$5	122
74	53	$\pm$5	103
63	44	$\pm$4	89
53	37	$\pm$4	76
45	30	$\pm$3	66
38	25	$\pm$3	57
25	20	$\pm$3	42

The aqueous fiber solution was first separated using the 90 μm sieve. Any material that did not fall through the sieve was collected and resieved a total of five times. The material that remained on top of the 90 μm sieve was discarded. The fibers that fell through the wire mesh were consequently sieved five times through the 74 μm sieve. This process was continued using the 63 μm, 53 μm, 45 μm, 38 μm, and 25 μm sieving. Sieved fibers from many millings and sievings were combined for further separation as discussed below.

The longest fibers were further classified by resieving them. This was done by sieving five times using the smallest sieve through which they had passed during the first separation to remove the long fibers followed by sieving five times using the largest sieve that they had remained on. The fibers separated using the 90 and 74 μm sieves were found to average 285 μm in length. Fibers beneficiated using the 74 and 63 μm sieves averaged 196 μm, those done with the 63 and 53 μm sieves averaged 166 μm, and the 53 and 45 μm sieves yielded and average length of 91 μm.

The second smallest aspect ratio of 4.2 beneficiated by suspending 2.5 g of fibers that had passed through the 25 μm sieve in 1 l of deionized water followed by multiple resedimentations. The suspension was allowed to settle for 55 minutes after which the top 900 ml of decant was discarded and the sediment was remixed with 900 ml deionized water for the next sedimentation stage. The material was sedimented four times at 55 min., 50 min., 45 min., 40 min., 35 min., 30 min., 25 min., 20 min., and 15 min for a total of 36 separate sedimentations during the secondary bonification. Decreasing the sedimentation time after each set of four runs was done to systematically eliminate the shorter fibers. This resulted in the production of approximately 0.25 g of 65 μm average length fibers.

Fractionation of the Lowest Aspect Fibers and the Particulate

The smallest aspect ratio of 1.3 used only vibratory ball milling and sedimentation to achieve the desired distribution. Five grams of fibers were vibratory milled using 300 g of SiC ball media and deionized water for four hours in a 250 ml Nalgene container. The fibers were sedimented six times for 60 minutes with 900 ml of decant being discarded while the sediment was remixed with water and resedimented. This resulted in the production of approximately 0.1 g of fibers that averaged 20 μm in length.

SiC particulate was also used to obtain a reasonable quantity of approximately equiaxed inclusions that were approximately the same size and shape as the smallest fibers. 600 grit SiC powder (PSI Testing Systems, Houston, Texas) was used in the as received form. It had a mean size of 12 μm and density of 3.18 g/cm^3 by helium pycnometry. The theoretical density of SiC is 3.21 g/cm^3 so the 600 grit powder is $\approx$99% SiC.

Characterization of the Fiber Distributions

The fiber distributions were characterized by optical microscopy. Three photomicrographs of separate batches of fibers from each distribution were analyzed. The length of 132 fibers was measured in each photomicrograph with digital vernier calipers. The mean, standard deviation, and coefficient of variation for each distribution are tabulated in Table II. The number frequency for each of the distributions are plotted in Figure 7.

Table II Statistical Description of the Fiber Distributions

Aspect Ratio	Mean Fiber Length (μm)	Standard Deviation of Lengths (μm)	Coefficient of Variation
600 grit	12	5	0.42
1.3	20	8	0.40
4.2	65	20	0.31
5.9	91	28	0.31
10.8	166	35	0.21
12.8	196	44	0.22
18.6	285	58	0.20

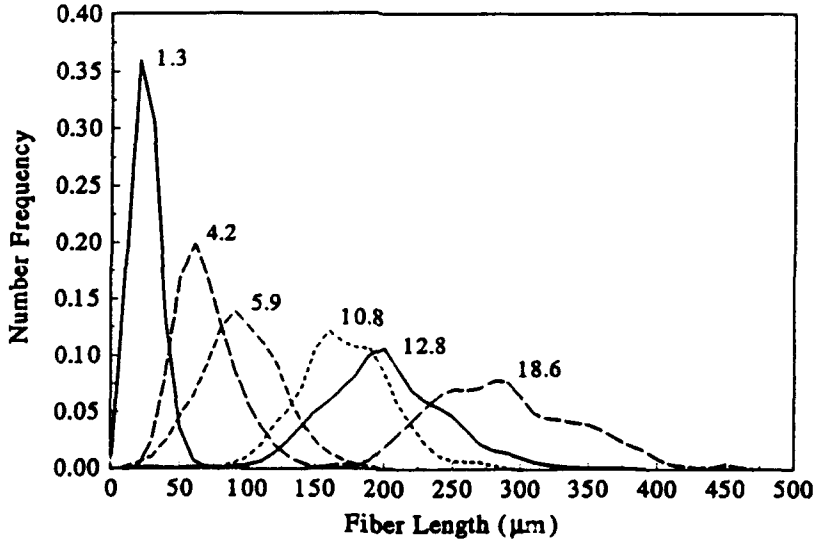

Figure 7 Frequency Distributions for the Six Different Aspect Ratios.

Examination of Figure 7 shows that the spread of the distributions increased as the mean length of the fibers increases. However, Table II shows that the coefficient of variation decreases as the mean fiber length is increased. Therefore, we believe that the primary difference between the distributions is their length and not their variability.

Figure 7 shows that there is a fair bit of overlap between the different distributions, particularly for those that are adjacent. It could probably be argued that there are really only four discrete fiber distributions (aspect ratios of 1.3, 4.2/5.9, 10.8/12.8, and 18.6) instead of the six that were fractionated. The green forming and sintering results tend to support this view part of the time, but there are enough differences that we will continue to treat them as separate distributions. Optical photomicrographs of the six fiber distributions are shown in Figure 8 and discussed below.

The fibers in the 1.3 aspect ratio distribution ranged from sub micrometer to approximately 70 μm. Vibratory milling longer than four hours eliminated most of the longer (>70 μm) fibers by chopping them into smaller ones, but it also produced many fiber particles that were very short. The six one-hour sedimentations were effective in removing most of the fibers less than 10 μm long, although many short and broken pieces of fiber remained. This micrograph also shows many short fibers that are broken longitudinally, along with pieces of fibers with no discernable aspect ratio. The combination of cylindrical fibers and roughly equiaxed particles is an interesting link between the 600 grit SiC powder distribution and the longer fiber distributions.

Sedimentation combined with sieving produced a fairly narrow 4.2 aspect ratio, although the distribution did trail off into the longer fiber lengths as shown in Figure 7. The micrograph in Figure 8 shows some small chips along with a few longer particles. The sedimentation process was fairly effective in removing the short fibers as shown by the steep positive slope on the short side of the frequency versus length distribution curve in Figure 7.

The four longest distributions are more symmetric than the two shorter distributions discussed previously. This indicates that sieving process is not as selective in fractionating the fibers by length. The micrographs in Figure 8 show that there are few very short shattered fibers in these distributions and that the fibers appear to have a uniform cross section.

Discussion of the Fractionation Process

Sedimentation produces narrower distributions with shorter tails than sieving. Unfortunately, sedimentation is a very inefficient process that only yields 4 to 10% when pushed to produce very narrow fiber distributions. Sieving wastes little product but the resulting distributions are much wider with much broader tails as shown in Figure 7.

During sieving, the fibers ideally flow smoothly onto the wire mesh so that long fibers span the wires while short ones fall through the sieve. Figure 9 shows the minimum and maximum theoretical lengths for a fiber to be supported on the sieve. The minimum fiber length will just span a single opening and must have a length of at least o + w, where o is the distance between wires and w is the diameter of the wire. The diagonal fiber in Figure 9 is the maximum length of fiber that might fall through the sieve if the fiber axis parallel to the sieve surface. This fiber

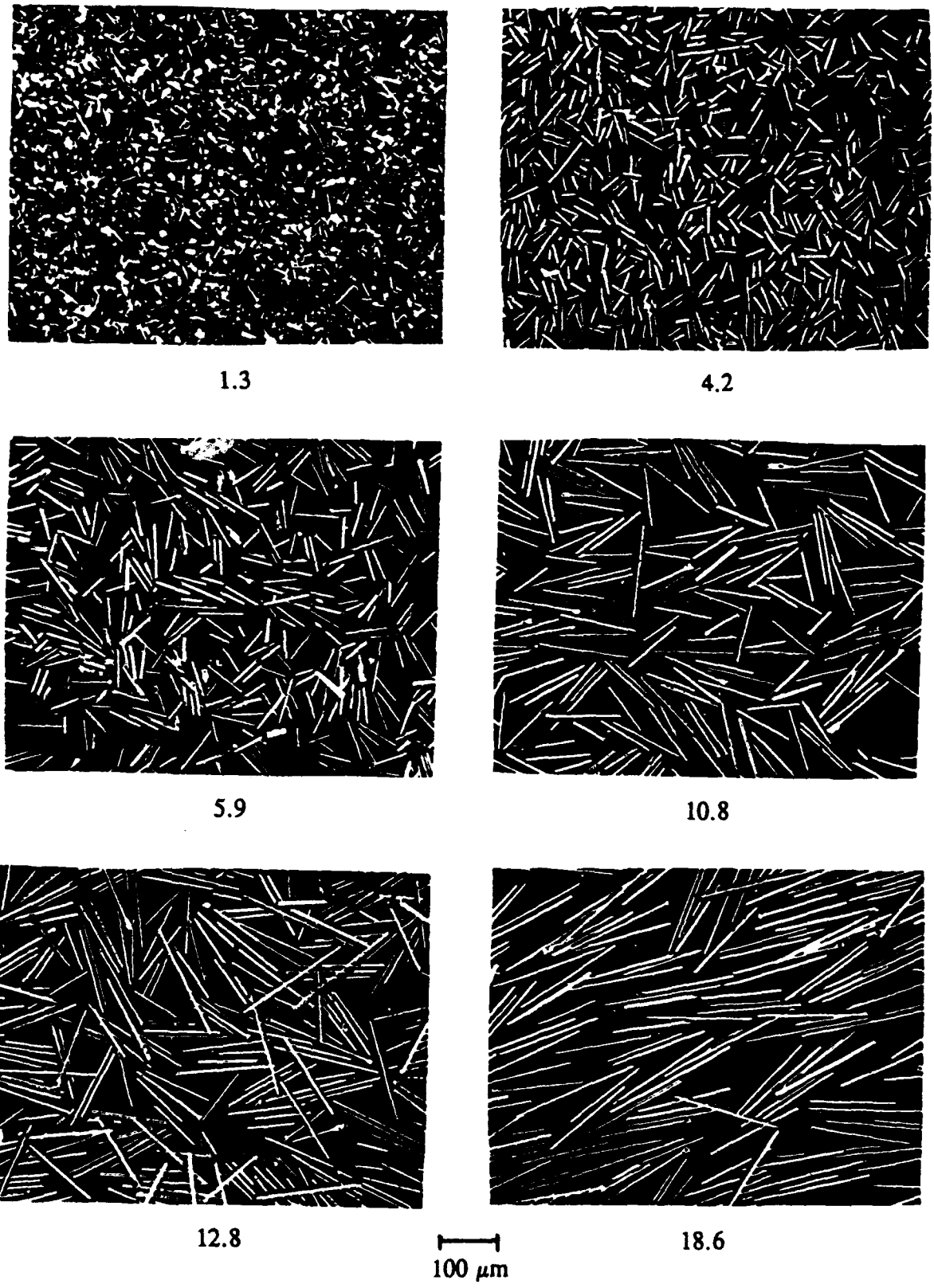

Figure 8 Optical photomicrographs of the six fiber distributions shown with a 100 μm marker.

has a length of $\sqrt{5w+4o}$ since it spans two openings and wires in one direction and a single opening in the other direction. Obviously longer length fibers would not pass through the sieve if they are properly oriented.

This model predicts that only fibers shorter then $\sqrt{5w+4o}$ may pass through a sieve while only those longer than o + w should be retained on the sieve. Table III lists both the theoretical and experimental fiber length ranges for each of the sieves employed in this study. The minimum theoretical and experimental fiber lengths agree reasonably well except for the smallest sieve indicating that this portion of the analysis is good. However, the experimental maxima are approximately 140% of the theoretical lengths indicating that fibers that should be retained by the sieve are passing through.

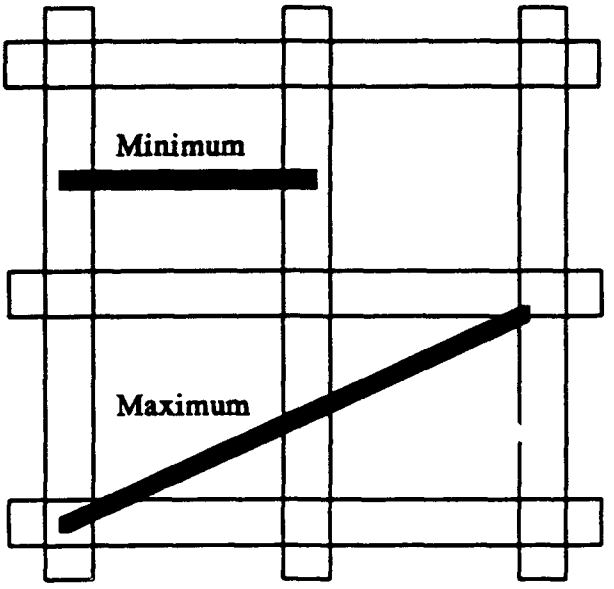

Figure 9 Maximum and minimum configurations that would prevent a fiber from passing through the wire mesh.

Table III *Theoretical and Experimental Fiber Lengths (μm) for the Different Sieves*

Sieve Opening (μm)	Wire Diameter (μm)	Theoretical		Experimental	
		Min	Max	Min	Max
90	64	154	344		460
74	53	127	284	150	
63	44	107	239		340
53	37	90	201	90	290
45	30	75	168	80	
38	25	63	141		190
25	20	45	101	10	

The poor agreement between the theoretical and experimental maximum fiber lengths may be a result of the fibers not sliding or rolling across the sieve cloth smoothly. Turbulence in the fluid flow and interaction with other fibers would cause the fibers to tumble. This would result in the fibers having a more vertical orientation that would allow some longer fibers to pass through the sieve. In addition, the surface of the sieve is not smooth since the sieve cloth is woven from wires. The wires are displaced vertically so that they can alternately pass above and below the wires that are oriented in the perpendicular direction. Therefore, the surface of the sieve undulates by approximately the wire diameter which will induce additional turbulence in the flow and cause the fibers to pass through the sieve.

The sieving process could be improved dramatically by using a perforated plate sieve rather than the woven wire sieves used in this study. These sieves are fabricated from thin metal plate in which holes are etched. In addition to eliminating the roughness due to weaving the wires, it is possible to create more uniform hole sizes since these sieves are produced by photolithography. The distribution of fiber lengths could be further improved by using a sieve with circular holes rather than square holes since the minimum fiber length that will be retained is then independent of the fiber orientation in the plane of the sieve. However, it is anticipated that this type of sieve will be less efficient than the woven wire sieves since a much smaller fraction of the sieve is perforated.

2.2.2 Composite Fabrication

Several different volume fractions from each SiC aspect ratio were fabricated into Al_2O_3/SiC pellets. For each aspect ratio and volume fraction, five pellets were formed by slip casting a suspension of Al_2O_3 and the SiC fibers in an acrylic mold on a plaster bat. Fine grained alpha alumina was used for the experiments (AKP-30, Sumitomo Chemical America Inc., New York, NY) with a mean particle size of 0.39 μm. It was selected because it was the easier to densify compared Sumitomo's AKP-15 and AKP-50 powders in a previous study[3] since it was fine enough to densify well but coarse enough for easy green processing. Table IV lists the aspect ratio and SiC volume fraction combinations that were fabricated in this study. The high volume fraction materials were not fabricated from several aspect ratios since it was not possible to fractionate enough SiC fibers of these aspect ratios.

Table IV The SiC_f aspect ratios and volume fractions used in the study

Aspect Ratio	Volume Fraction SiC						
	0.048	0.096	0.145	0.193	0.242	0.291	0.340
1.3	X	X	X				
4.2	X	X	X	X	X	X	
5.9	X	X	X	X	X	X	X
10.8	X	X	X				
12.8	X	X	X	X	X		
18.6	X	X	X	X	X		
600 grit*	0.400	0.810	0.123	0.166	0.210	0.255	0.300
	X	X	X	X	X	X	X

* The 600 grit SiC/Al_2O_3 composites were fabricated with lower SiC volume fractions because the particles and fibers were assumed to have the same density when the composites were made.

The alumina powder and SiC were mixed with deionized water and the suspension pH was adjusted to 4 with reagent grade nitric acid (J.T. Baker Inc., Phillipsburg, NJ). A pH of 4 was selected since both Al_2O_3 and oxidized SiC are stearically stabilized from a pH of approximately 3 to 5. Nitric acid was chosen because it leaves little or no residue during sintering. A Vibra Cell High Intensity Ultrasonic Processor (Sonics & Materials, Inc., Danbury, CT) was used to sonicate the slip four times for 1 minute at approximately 20 watts to break up any agglomerates. The mixture was shaken between sonications to ensure sonication of the material on the sides and in the cap. After sonication a Burrell Wrist Action Shaker (Burrell Scientific, Pittsburgh, PA) was used to shake the slip for 1 hour to ensure even distribution of the fibers throughout the alumina matrix. Careful mixing was important to avoid fiber segregation[4]. Following shaking the slip was placed under a vacuum for 10 minutes to remove air contained within the slip.

Pellets were then slip cast from the slurry in an acrylic mold which was tapered at 5° so that the top was smaller than the bottom. The pellets dried in the mold at room temperature for 24 hours, followed by oven drying at 90°C for an additional 24 hours. The pellets were trimmed to remove flash from the bottom of the pellet and the menisci from the top. The pellets had an average diameter of 12.7 mm and an average height of 5.5 mm. The green density was determined by measuring the top and bottom diameter along with the height to 0.01 mm, and the mass to 0.01 g.

The pellets were sintered in a Keith furnace (W.P. Keith Co., Inc., Pico Rivera, CA) at 1400°C in air for one hour with 5°C/min heating and cooling ramps. Sintered densities were determined by Archimedes' method using deionized water. The fractional green densities were calculated for both the green and sintered states using the theoretical density calculated from the density of Al_2O_3 (3.98 g/cm^3), SiC (2.6565 g/cm^3), and the initial composition of the composites.

2.2.3 Green and Sintered Composite Density

Green Densities

Table V and Figure 10 present the fractional green densities for the seven fiber aspect ratios and the 600 grit SiC powder. The green density of pure Sumitomo AKP-30 alumina compacts processing in the same manner as the composites was 0.639 ± 0.0062. This is approximately the overall mean for all of the composites.

Table V Green Density (top) and Standard Deviation (bottom) for the Composites Studied

Aspect Ratio	Volume Fraction SiC						
	0.048	0.095	0.145	0.193	0.242	0.291	0.340
1.3	0.634 0.0027	0.642 0.0031	0.636 0.0054				
4.2	0.623 0.0034	0.623 0.0069	0.638 0.0049	0.658 0.0020	0.650 0.0009	0.660 0.0062	
5.9	0.605 0.0034	0.631 0.0059	0.641 0.0061	0.646 0.0079	0.650 0.0063	0.686 0.0037	0.696 0.0039
10.8	0.639 0.0068	0.628 0.0045	0.628 0.0076				
12.8	0.634 0.0059	0.612 0.0042	0.631 0.0057	0.632 0.0096	0.666 0.0043		
18.6	0.613 0.0049	0.614 0.0055	0.623 0.0030	0.640 0.0066	0.646 0.0009		
Fiber Average	0.625	0.626	0.634	0.645	0.652	0.671	0.697
600 grit	0.400	0.810	0.123	0.166	0.210	0.255	0.300
	0.590 0.0108	0.631 0.0132	0.638 0.0194	0.651 0.0148	0.650 0.0151	0.666 0.0149	0.698 0.0060

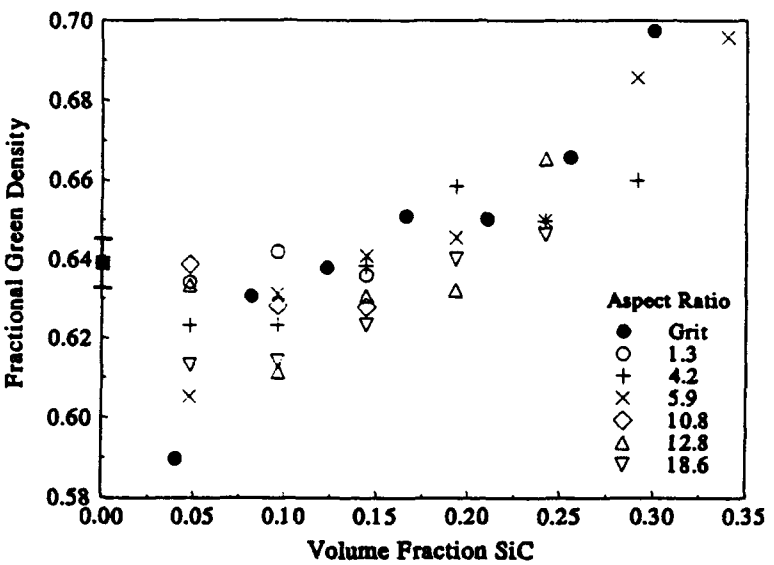

Figure 10 Composite green density as a function of volume fraction for the different aspect ratios. The behavior of the pure alumina is shown using a solid box with error bars.

Examination of Figure 10 shows that the green densities increase as volume fraction of SiC is increased. It is also seen that the green densities become more uniform as the volume fraction is increased. This is felt to be a consequence of the density being limited by packing considerations as the green density increases. However, it may also simply be an artifact of the smaller number of composites that were made at high volume fractions due to limited quantities of SiC fibers.

The effect of fiber aspect ratio on green density is shown in Figure 11. The green density appears to decrease slightly with increasing fiber aspect ratio. Least squares linear regression of the green density versus fiber aspect was performed for the 0.048, 0.096, and 0.145 volume fraction SiC fiber composites since all six aspect ratios were available at these compositions. The results of this analysis are shown in Table VI were it is seen that the green density decreases with increasing fiber volume fraction, but the correlation is weak at best. However, there does appear to be a consistent decrease in the variability of the green density as the volume fraction of inclusions is increased.

Table VI Regression Analysis of Green Density Versus Fiber Volume Fraction

Fiber Volume Fraction	Equation	R^2
0.048	$0.6275 - 0.00029\ f_{Fiber}$	0.019
0.096	$0.6380 - 0.00145\ f_{Fiber}$	0.660
0.145	$0.6411 - 0.00091\ f_{Fiber}$	0.744

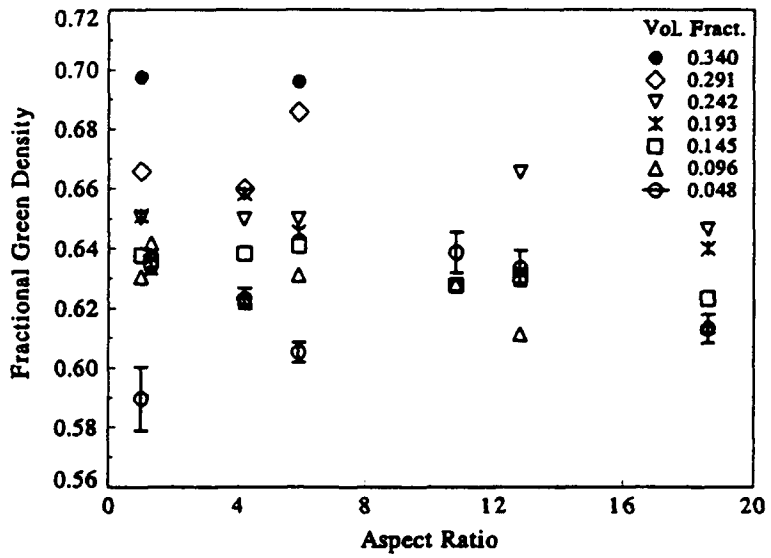

Figure 11 Composite green density as a function of inclusion aspect ratio for the different inclusion volume fractions.

Tseng and Funkenbusch[5] found increasing green density as a function of Si_3N_4 whisker volume fraction in slip cast Al_2O_3 matrix composites. Sacks *et. al.*[6, 7] found that the green density is relatively independent of whisker size and volume fraction of whiskers in slip cast Al_2O_3/SiC_w compacts. Tiegs and Dillard[8] found the green density decreased as the volume fraction of SiC whiskers was increased in Al_2O_3/SiC_w composites. Several investigators[5, 7, 9] have found that

increasing the volume fraction of SiC whiskers in dry pressed compacts decreased the green density.

The major difference between these studies and the current study is that fibers used in this study are significantly larger than the whiskers used in the other studies while the matrix powders are approximately the same size. The Furnas model[10] predicts that spherical binary mixtures with a large size ratio (>7) will pack more efficiently than either powder by itself since the small particles fill the interstices between the large ones. Messing and Onoda[11] have verified the Furnas relationship for ceramic powders in the same size ranges as those studied here, but point out that deviations from Furnas relationship may occur due to inhomogeneities in the binary compact. Many investigators have found that high quality green processing allows the particles to pack more efficiently. It is proposed that the combination of high quality green processing and a large size difference between the fibers and the matrix particles allowed the alumina particles to fill the interstices between the fibers resulting in the observed increase in green density with increasing fiber volume fraction.

The green density does not appear to depend strongly on the fiber aspect ratio which seems to rule out percolation effects since the longer fibers should be long enough for percolation to occur, particularly at the higher volume fractions. Holm and Cima[12] simulated percolation of fibers in a two-dimensional lattice and found that there should be very pronounced percolation effects at modest aspect ratios and volume fractions. The lack of percolation effects in the green compact is probably the result of good green processing and partial alignment of the fibers when the slip was poured into the mold. Good green processing will distribute the fibers throughout the slip and may have coated the fibers with a thin layer of matrix particles that would allow them to slide past each other during consolidation. The slips appeared to form streamlines when they were poured into the mold which would align the fibers and inhibit percolation effects. Examination of the microstructure of the fired composites showed that there were some regions where the fibers are aligned, but this was not quantified.

Fired Densities

The fractional sintered densities are listed in Table VII and shown in Figure 12 as a function of the fiber volume fraction and in Figure 13 as a function of the fiber aspect ratio. The AKP-30 Al_2O_3 used in this study sintered to a fractional density of 0.986 ± 0.0109 upon heating to 1400°C at 5°C/min with a one hour hold at temperature. As expected this is higher than any of the composites. However, several low volume fraction composites reached densities that were not statistically different from that of the pure alumina.

Table VII Fractional Fired Densities and Standard Deviations for the Composites

Aspect Ratio	Volume Fraction SiC						
	0.048	0.095	0.145	0.193	0.242	0.291	0.340
1.3	0.968 0.0092	0.941 0.0093	0.920 0.0033				
4.2	0.959 0.0088	0.961 0.0115	0.947 0.0080	0.942 0.0058	0.913 0.0075	0.885 0.0064	
5.9	0.983 0.0092	0.963 0.0091	0.936 0.0068	0.918 0.0102	0.894 0.0051	0.886 0.0030	0.866 0.0066
10.8	0.984 0.0089	0.975 0.0122	0.948 0.0118				
12.8	0.984 0.0091	0.969 0.0091	0.942 0.0142	0.885 0.0071	0.874 0.0097		
18.6	0.965 0.0053	0.933 0.0167	0.915 0.0081	0.878 0.0041	0.841 0.0094		
600 grit	0.040	0.081	0.123	0.166	0.210	0.255	0.300
	0.889 0.0278	0.862 0.0107	0.848 0.0173	0.838 0.0155	0.828 0.0052	0.811 0.0192	0.815 0.0225

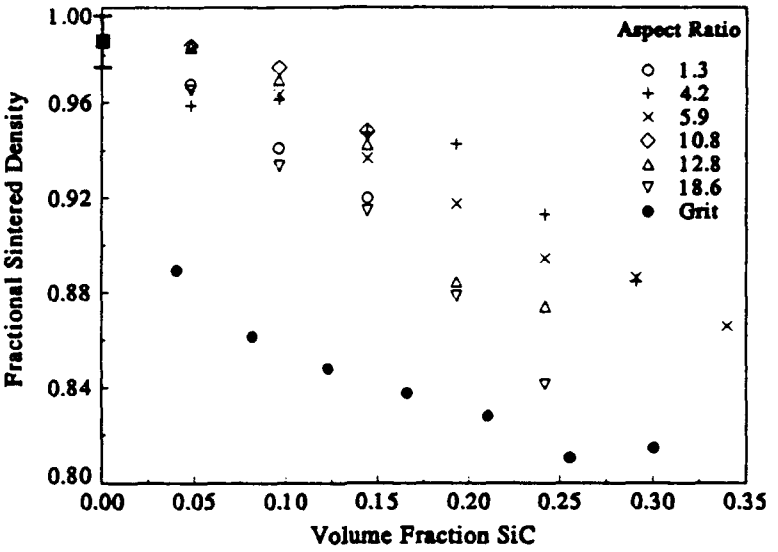

Figure 12 Sintered density of the composites as a function of volume fraction inclusions for the different aspect ratios. The behavior of the pure alumina is shown using a solid box with error bars.

As stated above, several low volume fraction composites sintered densities that are statistically the same as the pure alumina processed under the same conditions. Several previous studies have found low volume fractions of whiskers and fibers had little or no effect on the sintered density of the composites.[7-9] However, other investigators have seen an immediate decrease in sintered density at low inclusion fractions.[5, 7, 13] Differences in the green processing methods between these studies are the most likely cause of the differences in sintered density at low (<0.10) fractions of inclusions. The composites made using the 600 grit powder sintered to much lower densities and will be explained later in this section.

Figure 12 shows that the sintered density decreases dramatically as the volume fraction of fibers increases which is exactly the opposite trend seen for the green densities. This is the behavior that is observed in nearly every other study of solid state sintering of ceramic matrix composites. Three types of behavior are observed in Figure 12. The first is that the 600 grit SiC particulate composites did not densify nearly as well as the other composites. The second is that the density of the composites made using low and medium aspect ratio fibers (1.3 to 10.8) decreases linearly with increasing fiber volume fraction. Finally, the density of the composites made with long fibers decreases approximately linearly until a volume fraction of 0.15 when the density starts to decrease more rapidly.

Figure 13 shows the fractional sintered density as a function of fiber aspect ratio. The data for the 600 grit particulate and the 0.34 fiber volume fraction have been removed from this plot for the sake of clarity. The sintered densities reach a maximum at moderate aspect ratios (8-12) for the composites containing low volume fractions of fibers (<0.15). This is highlighted by the second order polynomials that were fit to these three data sets. It appears that the location of this peak shifts to lower aspect ratios as the volume fraction of fibers increases. At higher fiber

volume fractions (>0.15) the sintered density decreases with increasing fiber volume fraction. However, there may also really be a peak density at these higher fiber volume fractions that cannot be seen because there are not enough discrete fiber distributions at low aspect ratios.

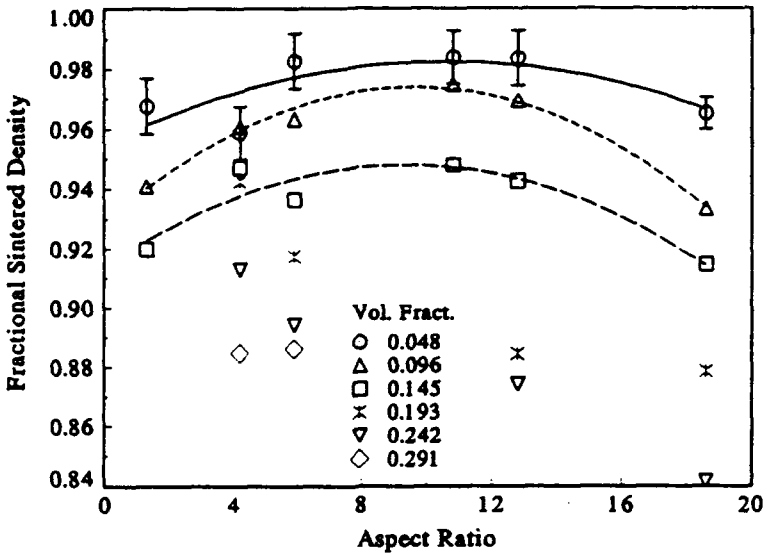

Figure 13 Sintered composite density as a function of aspect ratio for all volume fractions except 0.340. The data for the 600 grit particulate has been omitted to improve the clarity of the figure.

The density of the composites decreases strongly with increasing fiber volume fraction for all of the aspect ratios studied here. None of the aspect ratios exhibit the sharp drop off in the density that is indicative of percolation limited densification. This in spite of the fact that the combination of fiber volume fraction and aspect ratio should be high enough for percolation effects to occur. It appears that this densification behavior is best explained by the excluded volume effect described by Balberg[14] with a small contribution due to percolation. Tiegs and Dillard[8] studied the effect of SiC whisker aspect ratio on densification, but they only used volume fractions of 0.1 and 0.2, and did not see a critical volume fraction effect that would be indicative of percolation.

The densities of the low to moderate fiber volume fraction composites peaked at moderate aspect ratios of approximately ten. This peak in the sintered density at moderate aspect ratios suggests a transition region where fiber interactions begin to impede densification. It may be possible to take advantage of this effect to produce high density fiber reinforced ceramic matrix composites that have high fracture toughnesses. This is because moderate aspect ratio fibers should toughen the matrix via a variety of mechanisms including crack bridging, deflection, and pinning. Further improvements in the green processing may allow this peak in the sintered density to be pushed to higher aspect ratios and fiber volume fractions.

The composites made with the 600 grit powder did not densify nearly as well as those made from the Nicalon fibers. The 600 grit SiC powder averaged 12 μm in diameter and was therefore smaller than even the shortest aspect ratio fibers which were 15 μm in diameter and averaged 20 μm long. In addition, the 600 grit powder had many more very small particles, less than one micrometer, than the fiber distributions. Therefore, the surface area of the 600 grit powder is significantly higher than that of the Nicalon fiber distributions. Table VIII lists the surface areas

of the SiC particles and fibers calculated from the average sizes listed in Table II. The surface areas listed in Table VIII underestimate the actual areas since the distributions are represented by the average value. However, the surface area of 600 grit powder is underestimated by a larger amount than that of the fiber distributions since the very fine particles were not removed from this SiC powder.

Table VIII Calculated Surface areas for the Different Inclusions

Aspect Ratio	Mean Fiber Length (μm) (μm)	Average Surface Area (m^2/g)
600 grit	12	0.236
1.3	20	0.138
4.2	65	0.112
5.9	91	0.109
10.8	166	0.105
12.8	196	0.104
18.6	285	0.103

The poorer densification of the 600 grit composites is primarily due to inclusion surface area/size effects in which smaller inclusions inhibit densification more than larger ones as discussed by Weiser and De Jonghe[15] and Kimura *et. al.*[16] Densification is impeded because a layer of matrix particles adhere to the inclusion surface during sintering and increase the effective inclusion volume fraction. The effect is very pronounced for the 600 grit powder since the surface area is double that of the small fibers. This effect may also be responsible for the peak in the sintered density seen in Figure 13. This would be because densification is inhibited by surface area effects at low aspect ratios and by percolation related effects at high aspect ratios.

2.2.4 Microstructure of Fiber Reinforced Composites

One sample from each set of five pellets was sectioned axially and polished with a final step of 0.25 μm diamond. The microstructure of the samples was revealed by thermal etching at 1400°C for ten minutes. The polished and etched surfaces were examined using SEM at various magnifications. The chemical composition of the fiber/alumina interface was determined using Energy Dispersive X-ray Analysis (EDAX).

All of the composites exhibited relatively random inclusion distributions with some regions of uniform distribution and others where the inclusion distribution was either less than or greater than the average. The polished sections were examined along the pellet axis from the top to the bottom to determine if the heavier SiC fibers and particles had settled during slip casting. There was no evidence of sedimentation, although there was occasional fiber alignment as discussed above.

Moderate Aspect Ratios

Microstructures of the moderate aspect (4.2 and 5.9) ratio composites are shown in Figure 14 and Figure 15. The two micrographs in Figure 14 show composites made using 0.145 volume fraction of 4.2 aspect ratio fibers and 0.242 volume fraction of 5.9 aspect ratio fibers. The region of the 0.145 volume fraction composite pictured has a lower than average fiber concentration and is relatively dense with the fibers oriented nearly perpendicular to the surface. There are a few large pores that are as large as 5 μm across, but most of the matrix in this region is homogeneous and near theoretical density. There are 1 to 3 μm gaps at the fiber/matrix interface in these and nearly all of the other composites. This gap is primarily an artifact of the thermal etching procedure since it is rarely seen in polished surfaces that were not thermally etched. EDAX was used to investigate this region and it was found that a small amount of silicon had diffused into the alumina as will be discussed later.

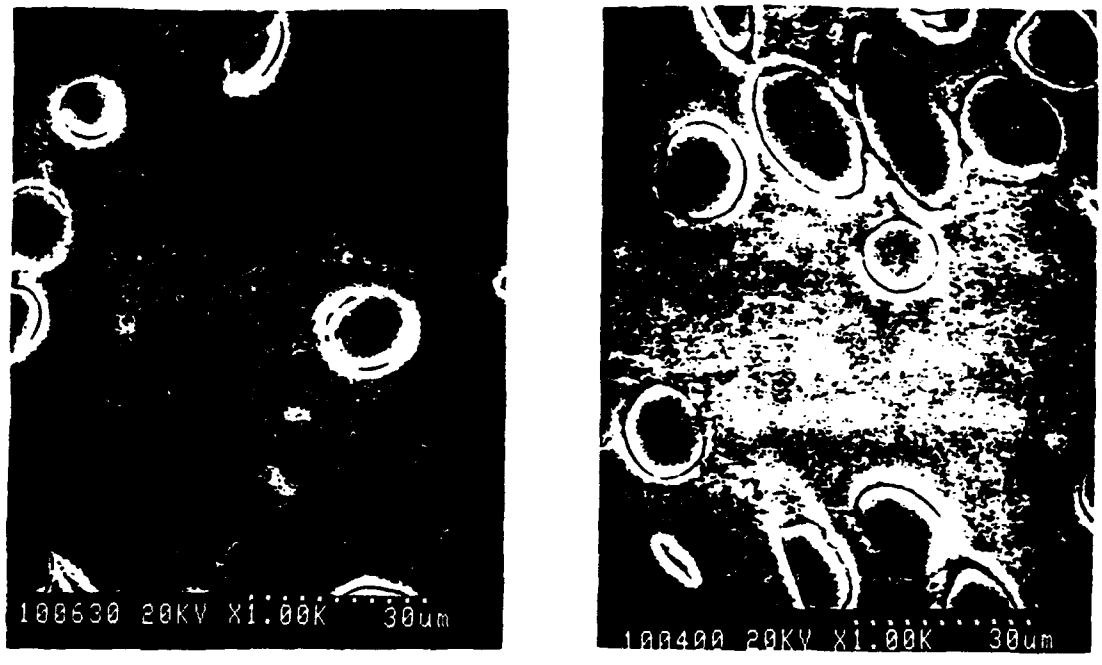

Figure 14 Polished and thermally etched surfaces of the composite made from 0.145 volume fraction 4.2 aspect ratio fiber (left) and 0.242 volume fraction 5.9 aspect ratio fibers (right).

The micrograph of the 0.242 volume fraction composite contains two regions of higher than average fiber concentration (top and bottom) with a region of nearly pure matrix between. The fibers in this micrograph are randomly oriented with both nearly perpendicular fibers (circular cross sections) and fibers that are oriented at a low angle to the surface (elliptical cross sections).

The central region of this micrograph is not particularly dense. This region contains both the large pores seen in the previous micrographs and much more fine porosity indicating that the matrix in this region did not densify very well. However, there are also regions of high density similar to those seen in the previous micrograph (upper and lower left) indicating that the extent of densification varies dramatically though the composite. It appears that the lack of densification in the central region cannot be explained based on simple constraint arguments since some of the densest regions in this micrograph are located at points where two and three fibers are within 10 to 20 μm of each other.

The surface of the composite made using 0.340 volume fraction 5.9 aspect ratio fibers is shown in Figure 15. The two lower magnification micrographs at the top of this Figure show that the high matrix density regions predominantly occur away from the fibers, while the regions near the fibers are relatively porous. The two lower micrographs show two different types of behavior in the central region of the low magnification micrographs which is surrounded by three fibers. In the lower left micrograph, a fiber is seen in the lower right corner of the micrograph and the upper portion is near theoretical density. The pores in this region are crack like and oriented radially away from the fiber indicating that hoop stresses that inhibit densification are probably present. The region shown in the lower right micrograph is located directly below the previous region such that they overlap slightly as seen by looking at the 0.4 $\times$ 1 μm pore at the matrix fiber interface. This region is located directly between two fibers that are only 4 μm apart and did not densify well. There is also a layer of matrix particles that adhered to the surface of the fiber along with a few large pores such as the one used above to align the micrographs.

High Aspect Ratio

Low magnification images of composites made with 0.242 volume fraction 18.6 aspect ratio fibers are shown in Figure 16. The matrix is composed of huge pores (up to 100 μm across) surrounded by relatively dense regions. However, this pellet had a high green density, which indicates that the pores formed during sintering rather than during green processing. The huge pores are probably the result of the formation of a percolation network of interlocking fibers that were unable to rearrange themselves during sintering. This prevented the alumina matrix from uniformly rearranging and shrinking so it broke apart in regions of relative weakness to form the huge pores. This was the only sample that exhibited such huge pores, but others displayed relatively large pores. We feel that this is because only this high volume fraction, high aspect ratio pellet had sufficient fiber interlocking for percolation to be very evident. It appears that percolation helps impede to densification at lower volume fractions and fiber aspect ratios, but the effect is not as dominant under these conditions as it is for this composite.

600 grit SiC Powder

The microstructures of the composites made using 600 grit SiC powder in Figure 17 is quite different from those of the fiber reinforced composites discussed earlier. The SiC particles are much more angular and more numerous since the particles are smaller. There is also a significant amount of porosity distributed through out the matrix, although there are regions of high density. The gaps between the matrix and the SiC particles are larger than those in the fiber reinforced composites. In the particulate composites this gap probably formed during sintering as

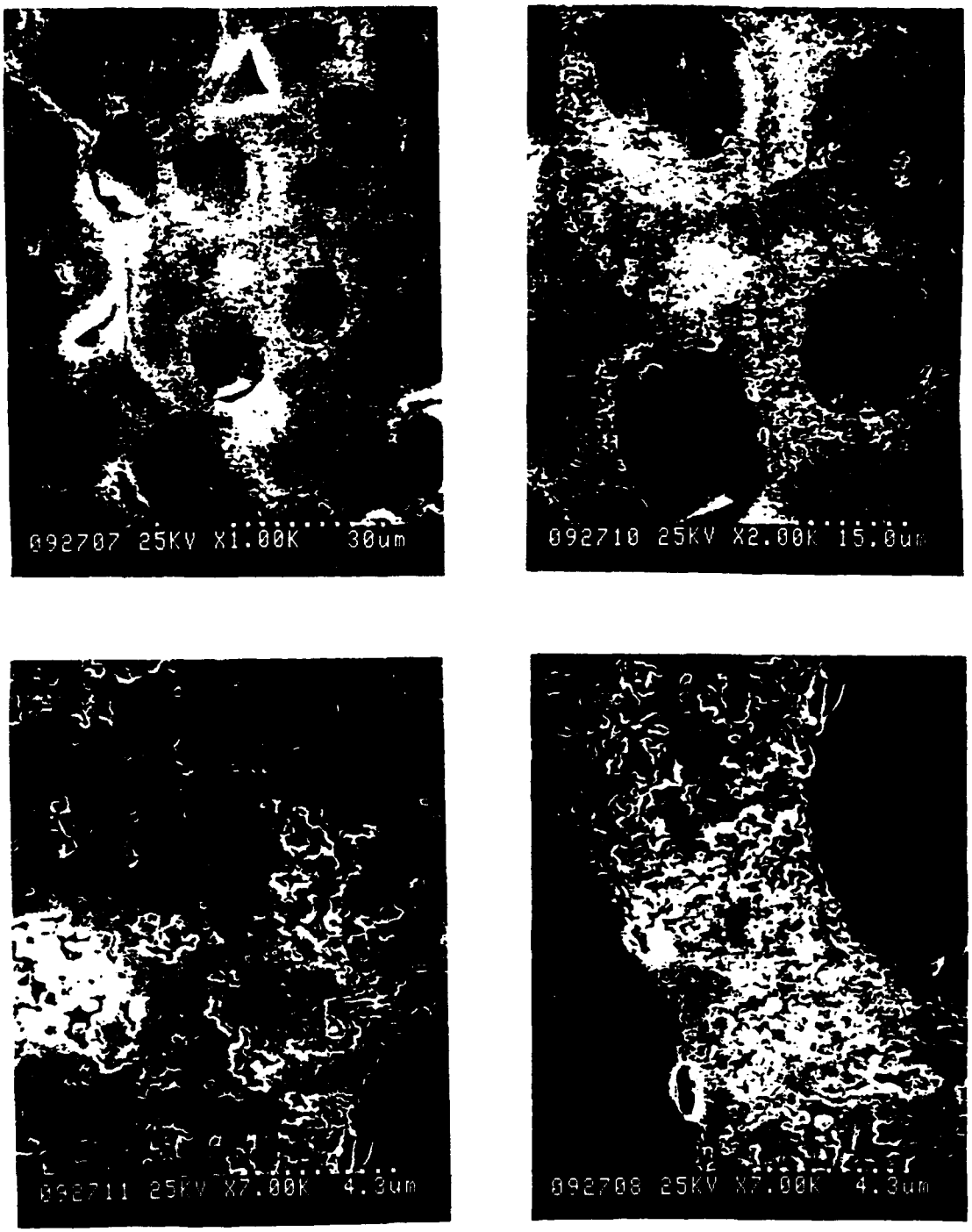

Figure 15 Polished and etched surface of the composites made using 0.34 volume fraction of 5.9 aspect ratio fibers.

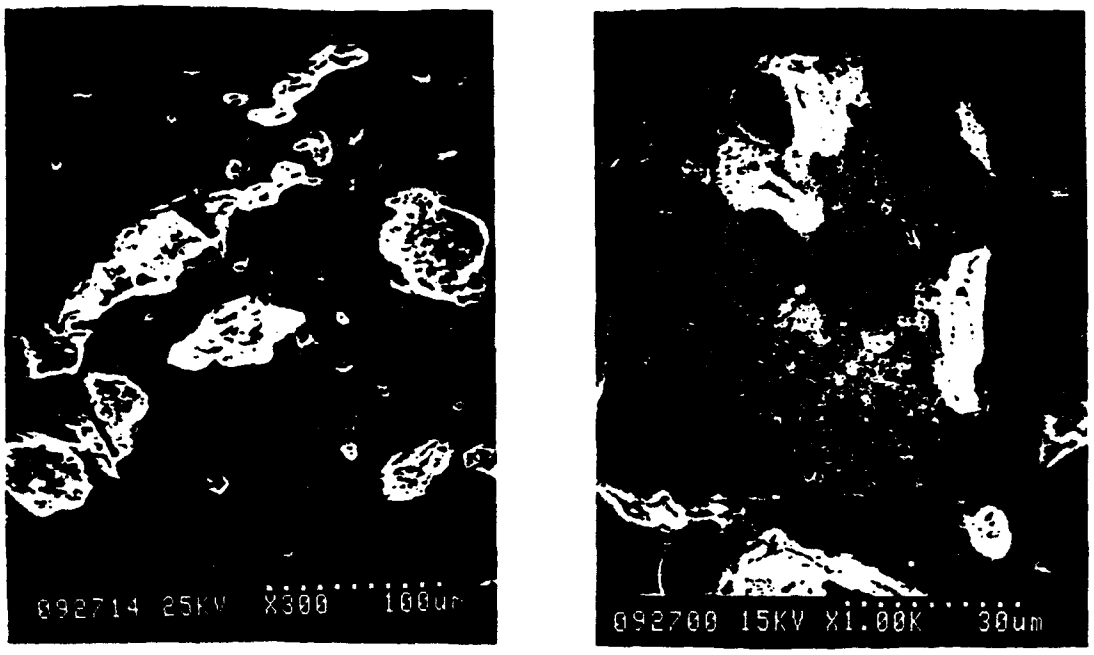

Figure 16 Polished and thermally etched surfaces of a composite made using 0.242 volume fraction fibers with an aspect ratio of 18.6.

well as during thermal etching since the nearly pure SiC particulate is not as well protected from oxidation as the Nicalon fiber which contains a significant amount of SiO_2.

Fiber/Matrix Interface

High magnification micrographs of the alumina matrix both close to and away from a fiber are shown in Figure 18. These micrographs happen to be from a composite made using 0.048 fraction of fibers with an aspect ratio of 18.6, but similar microstructures are seen in other composites. The left-hand micrograph shows a typical high density alumina microstructure with equiaxed grains that average 0.7 μm across. The right-hand micrograph shows the fiber/matrix interface. It shows that sintering and grain growth are strongly inhibited to a distance of about 1.5 μm from the fiber. EDAX revealed small amounts of silicon diffusion into the alumina matrix in this region with negligible silicon beyond 1.5 μm from the fibers. Impeded grain growth and diffusion of silicon into the matrix next to the inclusions was seen in all of the composites.

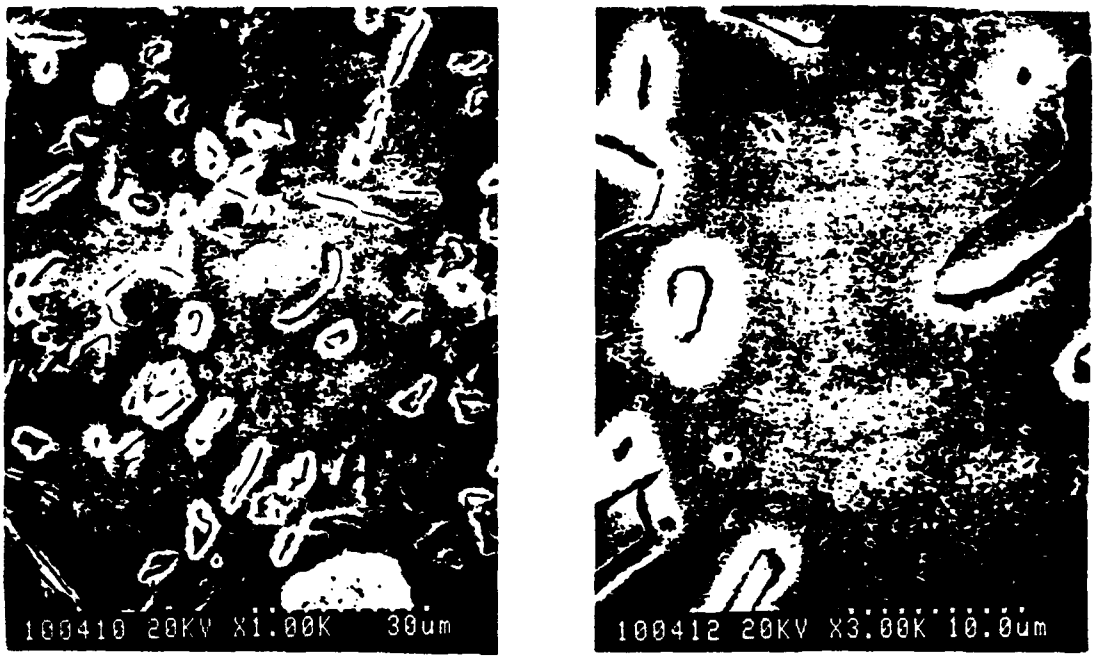

Figure 17 Polished and thermally etched surfaces of the composites made using 0.242 volume fraction of 600 grit SiC.

The silicon that diffused into the matrix around the particles could react with the alumina in several different ways. The silicon could combine with the alumina and any impurities to form low melting aluminosilicate glasses that result in transient liquid phase sintering. This should enhance sintering and densification, but this does not seem to be the case in these composites. The silicon could also combine with the alumina to form mullite which is very difficult to sinter. However, the observed silicon concentrations were never high enough to demonstrate mullite formation and X-ray diffraction (XRD) was not performed to check for mullite. The most likely scenario is that the silicon formed an aluminosilicate grain boundary phase (possibly mullite) that impeded grain growth and densification.

2.3 Aspect Ratio Conclusions

This study examined the effect of different volume fractions and aspect ratios of SiC fibers on the densification of an Al_2O_3/SiC_f composite. The objective of the study was to better understand the mechanisms by which fibers impede densification in fiber reinforced ceramic composites. It was hoped that there would be a clear break in the behavior as the volume fraction and/or aspect ratio was increased that indicates a change of mechanism. Such a break was not found, rather it was

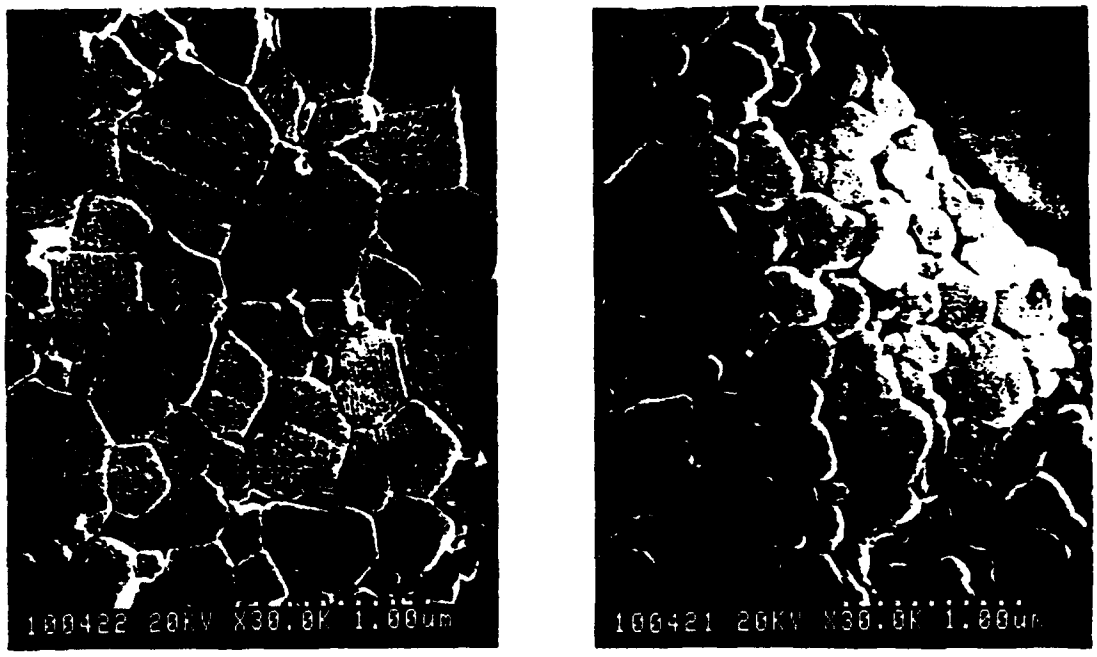

Figure 18 High magnification images of the polished and thermally etched surface of the 0.048 volume fraction, 18.6 aspect ratio composite.

found that there was gradual shift in the relative importance of each mechanism as the fiber volume fraction and aspect ratio were increased. Fractional sintered densities over 0.96 were obtained for composites made from low volume fractions of moderate aspect ratio fibers. This in spite of the fact that the composites were only sintered for four hours at 1400°C. The relatively high sintered densities and lack of a distinct change in mechanism are attributed to high quality green processing that prevented the formation of flaws in the green bodies.

The fractional green density of the composites increased systematically from 0.60 to 0.69 as the volume fraction of inclusions was increased. This is attributed to the effective green processing methods used to form the slips that allowed the particles to pack efficiently. The green densities were relatively independent of the inclusion aspect ratio with a slight trend toward smaller scatter at high aspect ratios. This suggests that percolation effects did not occur during green processing.

The fractional sintered densities ranged from 0.81 to over 0.98 and decreased as the volume fraction of inclusions was increased. The composites made using the 600 grit SiC densified significantly less well than the fiber reinforced composites which is attributed to the smaller size and different chemistry of the powder. Fiber aspect ratio had a small effect on the sintered

density below a volume fraction of 0.15. There is a volume fraction dependent peak in the sintered density that is probably a transition from local to global constraint of densification. At volume fractions greater than 0.19 the sintered density decreases with increasing aspect ratio. However, there may be a peak in the density at low aspect ratios that was not seen due to the lack of data in this region.

There are several mechanisms that impede densification in the fiber reinforced composites. The first is locally constrained densification which occurs when the matrix particles near the inclusion surface are prevented from densifying. Stresses develop around the inclusions that compress the matrix particles in the radial direction and prevent them from rearranging in response to the tensile hoop stresses. In addition, silicon diffuses into the matrix from the SiC inclusions which chemically impedes grain growth and densification. This results in a 1.5 μm thick region of small poorly sintered alumina grains around the SiC inclusions. Besides resulting in low density inclusion/matrix interfaces, local constraint increases the apparent inclusion volume fraction since the layer near the inclusion is effectively part of the inclusion. This effect becomes larger as the inclusion size decreases and explains the poorer densification of the composites made with small aspect fibers and the 600 grit SiC powder which was significantly smaller than the fibers.

Global constraint occurs when networks of the nondeformable inclusions prevent long range rearrangement of the matrix particles. As the compact sinters it becomes very difficult for the large rigid inclusions to slide past one another to accommodate the strains imposed by densification of the fine matrix particles. The importance of this effect increases with increasing inclusion volume fraction and aspect ratio. Increasing the volume fraction causes the inclusions to be closer together so there is less matrix between them that can shear to accommodate the shrinkage strains. Increasing the aspect ratio causes the inclusions to interact with more inclusions. The extreme case of this is the formation of a nondeformable percolation network that is predicted to give a sudden dramatic decrease in the densification above the percolation threshold. None of the composites studied here exhibited a percolation threshold, but percolation effects related to globally constrained densification were observed. The highest combination of fiber volume fraction and aspect ratio studied here exhibited formation of huge pores that are indicative of percolation.

In conclusion, it appears that there are several mechanisms that impede densification of fiber reinforced ceramic matrix composites. Local constraint results in the formation of a region of matrix particles which adhere to the inclusion and densify poorly and increase the effective inclusion volume fraction. Global constraint prevents rearrangement of the inclusion network and is a "softer" form of percolation. The quality of the green processing is very important in pressureless sintering of ceramic matrix composites. High quality green processing leads to much higher sintered densities than those observed by previous investigators at moderate fiber volume fractions and aspect ratios.

3 Inclusion Distribution

Current densification theory of ceramic Matrix composites (CMCs) is based upon perfectly homogeneous distributions of the second phase although work has recently been published which indicates that inhomogeneities in the inclusion distribution cause much of the observed impediment of densification. Our study intends to develop a model for the densification of ceramic matrix composites containing an inhomogeneous distribution of rigid inclusions. The current study is being conducted to experimentally determine the effect of inhomogeneous inclusion distributions on sintering and densification. The primary objective will be to determine how known inhomogeneities in the inclusion distribution affect the densification behavior of Al_2O_3/SiC and Al_2O_3/ZrO_2 composites. This will allow the current homogeneous second phase distribution models to be modified to take these effects into consideration.

3.1 Description of Inclusion Distributions

Three different types of inclusion clustering, designated as size, amplitude, and concentration were examined in this study. These different types of inclusion clustering were accomplished by combining different volume fractions of granules that contained a low volume fraction of SiC with granules that contain a high volume fraction of SiC. A bulk inclusion concentration of 12 vol% was selected because it was high enough to have a significant impact on the densification behavior while permitting enough densification so that the effect of different types of clustering could be seen. In addition, 12 vol% inclusions should be close to the percolation limit since the SiC inclusions are approximately equiaxed. Therefore, the low concentration granules should densify quite well and the high concentration granules should densify quite poorly.

The three types of clustering examined here are shown schematically in Figure 19. The inclusion concentration in all of the drawings in Figure 1 is 12 vol% as it is in the composites studied here. Figure 19a shows a composite made from homogeneous 12 vol% granules. The distribution of inclusions in this composite should be similar that in a composite made from a well dispersed powder mixture. Amplitude inhomogeneity is shown in Figure 19b where the inclusions have been partitioned between low concentration and high concentration granules. A less severe form on amplitude inhomogeneity is shown in Figure 19c where the low concentration granules contain a small amount of SiC. Concentration inhomogeneity is illustrated in Figure 19d where most of the inclusions have been concentrated in a small fraction of the granules while the remaining granules contain a small volume fraction of inclusions. This is in contrast to Figure 19c where the inclusions are much more uniformly distributed.

Amplitude and concentration clustering are related by the need to maintain constant total inclusion volume fraction among the composites. The bulk composition of 12 vol% SiC was achieved by using different proportions of low concentration and high concentration granules. The composition of the low concentration granules, f_L, the composition of the high concentration

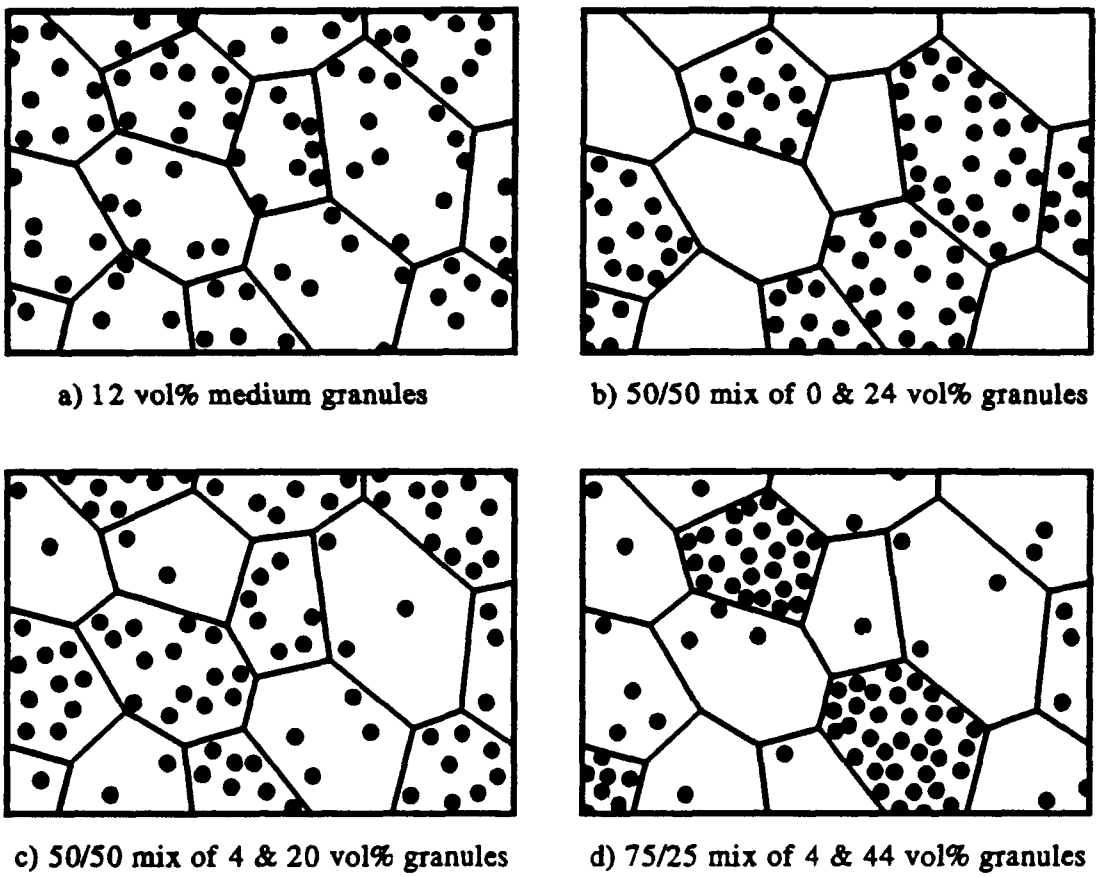

a) 12 vol% medium granules

b) 50/50 mix of 0 & 24 vol% granules

c) 50/50 mix of 4 & 20 vol% granules

d) 75/25 mix of 4 & 44 vol% granules

Figure 19 Schematic representation of the different types of inclusion inhomogeneity discussed in this paper.

granules, f_H, and the volume fraction of high concentration granules, F, are related to the bulk composition, f_B, by

$$f_B = Ff_L + (1-F)f_H \qquad 1$$

3.2 Al_2O_3/SiC Particulate Composites

3.2.1 Experimental Procedure

Four different volume fractions of high concentration granules, F, and three different compositions of the low concentration granules, f_L, were investigated in this study. This gives twelve different types of composites as listed in Table IX. The compositions of the low concentration granules are listed across the top of this table and the compositions of the high concentration granules is given in the body of the table. Careful selection of f_B, F, and f_L results in only eight different high concentration compositions. All 12 pellet compositions listed in

Table IX were fabricated from each of the four different sizes of granules. A series of pellets were also made from 12 vol% granules as a control to allow separation of the inclusion clustering effects from those due to granulation and dry pressing.

Table IX Granule Compositions and Volume Fraction

F	0	4	8
0.50	24	20	16
0.33	36	28	20
0.25	48	36	24
0.20	60	44	28

Inhomogeneous Al_2O_3/SiC composites containing a constant 12 vol% SiC were fabricated by dry pressing Al_2O_3/SiC composite granules of various sizes and SiC concentrations as listed in Table I to a green density of ≈ 50 to 54 %theor. The granules were made by slip casting well dispersed slips composed of 0.68 μm Al_2O_3 (AKP-15, Supplied by Sumitomo Chemical Co.) and 4 μm SiC particulate (Supplied by Norton Co. and air classified for a previous study[15]) using 0.25 vol% Na-PAA (Daxad 27, Supplied by W.R. Grace & Co.) as a dispersant[6, 17]. The slip cast composites contained from 0 to 60 vol% SiC and were granulated using a mortar and pestle. The granules were then sieved to obtain fractions of different granule sizes denoted as large (300-600 μm) medium (150-300 μm), small (75-150 μm), and very small (38-75 μm).

Composites were made from the granules by thoroughly dry mixing the proper volume fractions of granules (measured by mass) and uniaxial dry pressing. The pellets were pressed to nearly constant density by pressing a constant mass of powder to constant volume. The green pellets were 9.52±0.03 mm in diameter and 7.93±0.18 mm long and weighed 1.221±0.012 g. After dry pressing the pellets were sintered in air at 1450°C for 4 hours with 5°C/min heating and cooling ramps.

The density was computed from the pellet mass and dimensions since the pellets remained right circular cylinders during processing. The fractional matrix density is used in this study and was calculated using the following formula

$$\rho_{m,f} = \frac{m_{tot} - m_{incl}}{v_{tot} - v_{incl}} \times \frac{1}{\rho_{Al_2O_3}} \qquad 2$$

where m and v are the mass and volume of the entire pellet ($_{tot}$) and the inclusions in the pellet ($_{incl}$). The density of Al_2O_3 was taken to be 3.98 g/cm^3. All of the pellets except those made from pure Al_2O_3 exhibited a small weight gain upon sintering. The average weight gain for all of the pellets containing 12 vol% SiC was 0.028±0.003 g after correction for burnoff of the Na-PAA dispersant. This change in mass was assumed to be a result of oxidation of the SiC according to

$$SiC + 2\,O_2 \rightarrow SiO_2 + CO_{2\,(g)} \qquad 3$$

The volume of the inclusions after firing was corrected based upon oxidation of the SiC according to Equation 3. This resulted in an increase in the average inclusion volume from 0.038±0.000 cm^3 to 0.059±0.002 cm^3. It is entirely possible that mullite or other

alluminosilicates were formed which would give a slightly different inclusion volume after firing. However, the oxidation mechanism should be fairly constant for all of the samples containing 12 vol% SiC so the results will be consistently shifted.

3.2.2 Results

The matrix densities for all of the samples studied here are summarized in Table X. The composites containing SiC inclusions all densified significantly less than pure alumina. Pure alumina pellets reached 0.888 of theoretical density, while the final matrix density of the composites ranged from 0.571 to 0.699 of theoretical. The average clustered and homogeneous composites containing 12 vol% SiC had approximately the same initial ($\approx$0.53) and final ($\approx$0.66) matrix densities. However, the density of the clustered samples was much more broadly spread with a maximum matrix density of 0.739.

Table X Summary of the Matrix Densities

Pellet	# of Pellets	ρ_o	ρ_f	$\Delta\rho/(1-\rho_o)$
Clustered				
Average	136	0.523	0.661	0.291
Minimum		0.496	0.613	0.217
Maximum		0.543	0.739	0.429
Homogeneous				
0 vol% SiC	2	0.540	0.888	0.756
4 vol% SiC	2	0.537	0.699	0.349
8 vol% SiC	2	0.536	0.670	0.290
12 vol% SiC	12			
Average		0.533	0.657	0.267
Minimum		0.507	0.623	0.235
Maximum		0.540	0.667	0.275
16 vol% SiC	1	0.527	0.683	0.330
28 vol% SiC	1	0.515	0.639	0.255
36 vol% SiC	1	0.496	0.601	0.209
44 vol% SiC	1	0.452	0.571	0.217

There was a small systematic shift in the green density of the clustered composites during the study. The normalized matrix densification, $\Delta\rho/(1-\rho_o)$, will be used to compare the results from now on since it accounts for this shift. The normalized matrix densification of the pellets made from a single SiC concentration is shown in Figure 20. There are four separate data points at 12 vol% SiC although it appears that there are only two. This is because three of the different granule sizes behaved nearly identically. The addition of SiC dramatically decreases densification

under the sintering conditions employed here. The densification was modelled using the power law below

$$\frac{\Delta \rho}{1 - \rho_o} = 0.2146 f_{SiC}^{-0.1123} \qquad 4$$

with $R^2 = 0.895$ where f_{SiC} was set to 10^{-6} for the pure alumina compacts so the equation could be fit. The 95% confidence intervals are also plotted in Figure 20 showing that the model fits all of the data.

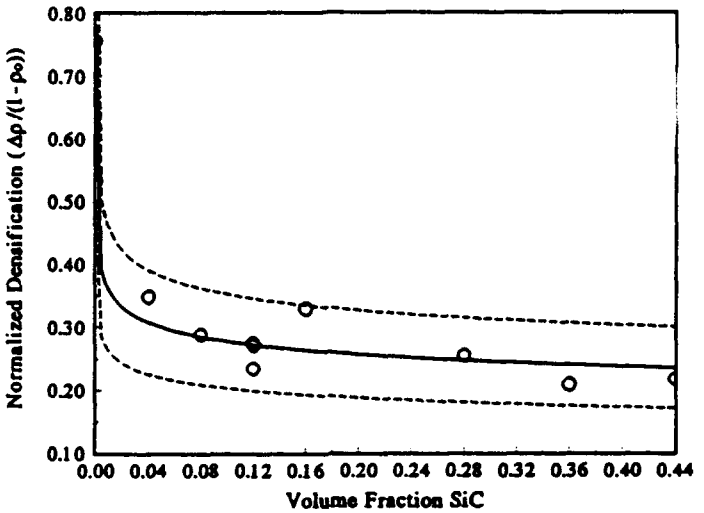

Figure 20 Normalized matrix densification for the limited number of homogeneous pellets available. The curve is a simple power law regression with 95% confidence intervals.

The microstructure of a typical series of clustered composites is shown in Figure 21. These dark field optical micrographs of polished surfaces show the distribution of the regions of high and low SiC concentration. It is seen that the regions are relatively uniformly distributed and that there is little or no cracking between the regions of high and low SiC concentration based upon strong differential densification of various regions as discussed by others.[18] The composites were examined in more detail using SEM and it was found that there were a few small microcracks between granules in the most heterogeneous composites.

The densification behavior of the clustered samples versus the average granule size is shown in Figure 22. Three sets of curves are shown in this Figure. The composites in the upper set of four curves (dashed lines) were made using low concentration granules that were made from pure alumina. The lower four curves (dotted lines) are for composites where the low concentration granules contained 8 vol% SiC. The solid line shows the behavior of the homogeneous compacts made from granules containing 12 vol% SiC. The results for the 4 vol% SiC low concentration composites are not shown, however, they fall between the 0 vol% and 8 vol% data. Typical error bars shown for the composites made using 20 vol% high concentration granules containing 60 vol% SiC and 80 vol% low concentration granules containing no SiC.

Composites made from the 0 vol% SiC low concentration granules densified much more than those made from the 8 vol% SiC low concentration granules. The densification behavior of these

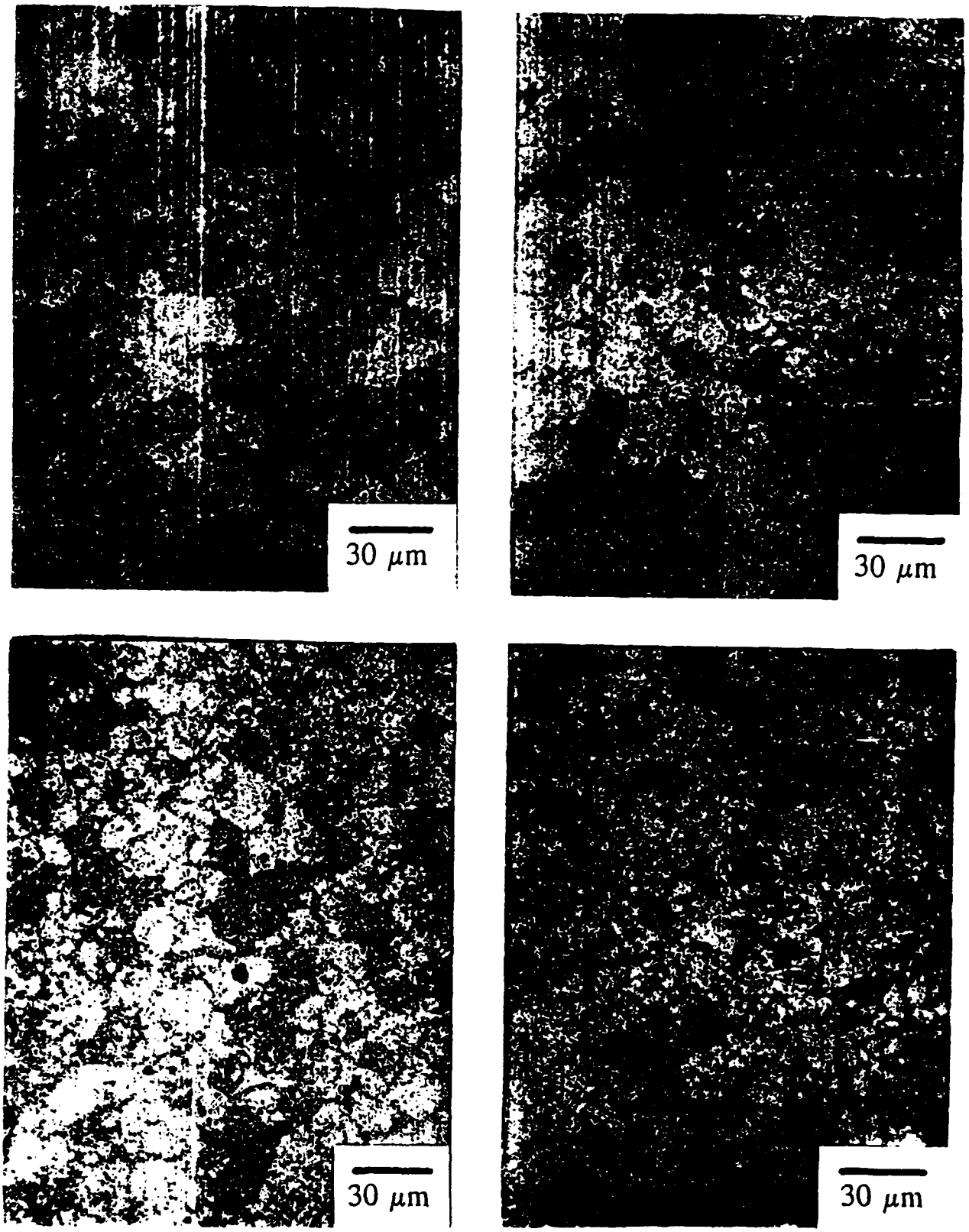

Figure 21 Dark field optical micrographs of clustered composites after firing made from medium granules. From upper left to lower right 0 and 24 vol% SiC, 0 and 36 vol% SiC, 0 and 48 vol% SiC, and 0 and 60 vol% SiC granules.

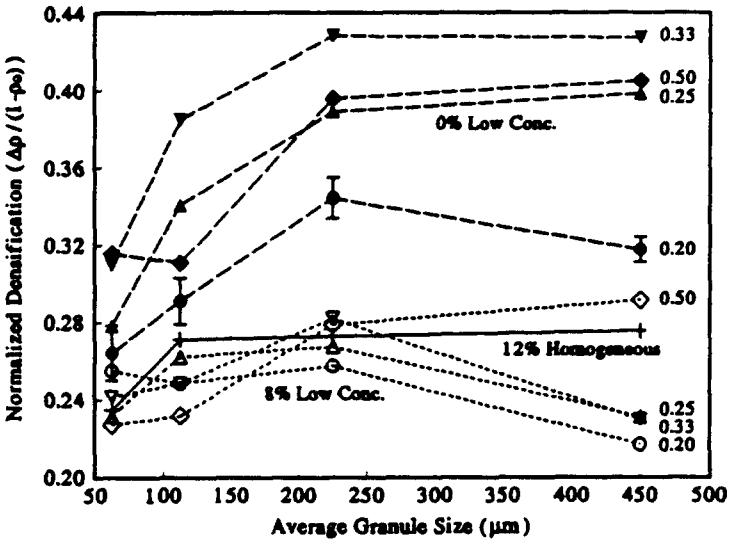

Figure 22 Normalized matrix densification versus the average granule size for the clustered composites and the homogeneous 12 vol% samples. Typical error bars are shown for the composites made from 0 and 60 vol% SiC granules.

more heterogeneous composites also strongly depends upon the fraction of high concentration granules and the granule size. The composites made from 0 vol% SiC low concentration granules all densified better than the homogeneous compacts while, for the most part, those made using low concentration granules containing 8 vol% SiC densified less. This suggests that strongly segregating the SiC inclusions into regions of high and low concentration increases densification while weakly segregating them decreases densification slightly.

The effect of the volume fraction of high concentration granules is shown more clearly in Figure 23. This figure plots the normalized matrix densification versus the volume fraction of high concentration granules at two of the four different granule sizes and all three low concentration granule SiC contents. The data for the medium and small granules is similar and lies between that of the large and very small granules. More heterogeneous composites made with low concentration granules containing small amounts of SiC and from larger granules densify better than those using small low concentration granules containing large amounts of SiC. The best densification is obtained when there is approximately the same volume fraction of low and high concentration granules.

The effects of all three parameters are summarized in Figure 24. This figure shows the densification behavior as a function of the average granule size and the volume fraction of high concentration granules for two of the three different low concentration granule compositions. The top surface is derived from the data for composites made from 0 vol% SiC low concentration granules while the lower surface is for the composites made with low concentration granules containing 8 vol% SiC. As discussed above, the composites made from purer low concentration granules densify much better than those made using low concentration granules that contained SiC. The best densification occurs for intermediate values of the other two parameters, granule size and concentration. The maximum densification is found to occur at 35 vol% of 170 μm high concentration granules for the 0 vol% SiC low concentration composites, 35 vol% of 170 μm high concentration granules for the 4 vol% SiC low concentration composites (not shown), and

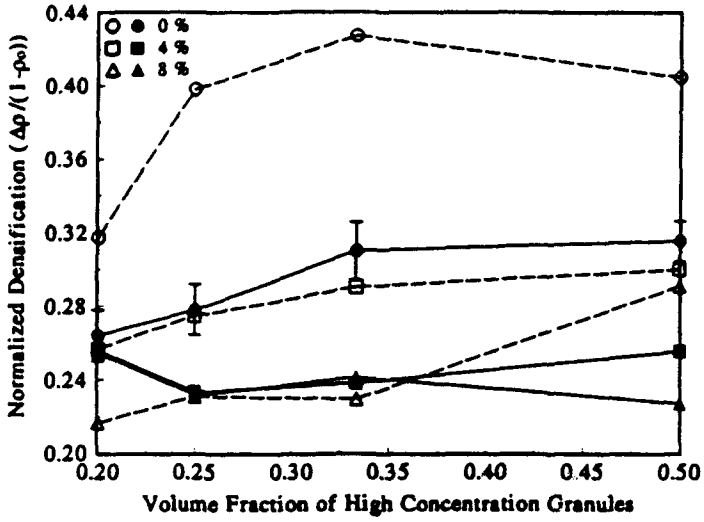

Figure 23 Normalized matrix densification versus volume fraction of high concentration granules for the large (empty symbols) and very small (solid symbols) granules.

38 vol% of 230 μm granules for the 8 vol% SiC low concentration composites. Although it is not shown for the sake of clarity the surface for the 4 vol% SiC low concentration granules looks a lot like a weighted average of the other two surfaces ($\approx$75% of the 8 vol% surface and $\approx$25% of the 0 vol% surface).

3.2.3 Discussion

It is clear from the data presented above that the moderately heterogeneous composites densify better than more homogeneous materials for the three types of inhomogeneity studied here. The major deviation from this finding is that the composites with the greatest difference between the SiC content of the high concentration and low concentration granules densified far better than those that were more homogeneous. It was found that somewhat inhomogeneous composites densify much better than those that are very homogeneous in this system. This finding could be used to improve the pressureless sintering of Al_2O_3/SiC_p composites. However, the authors feel that this degree of inhomogeneity will probably diminish the physical properties of the composite. On the other hand, recent studies have shown that very high fracture toughnesses are possible for inhomogeneous distributions of ZrO_2 in Al_2O_3.[19]

The better densification of the moderately heterogeneous composites compared to the homogeneous compacts and the very heterogeneous composites can be explained based upon local constraint of matrix densification.[20] In this model, a layer of matrix particles at the surface of the inclusion particles is constrained from densifying by the non-deformable nature of the

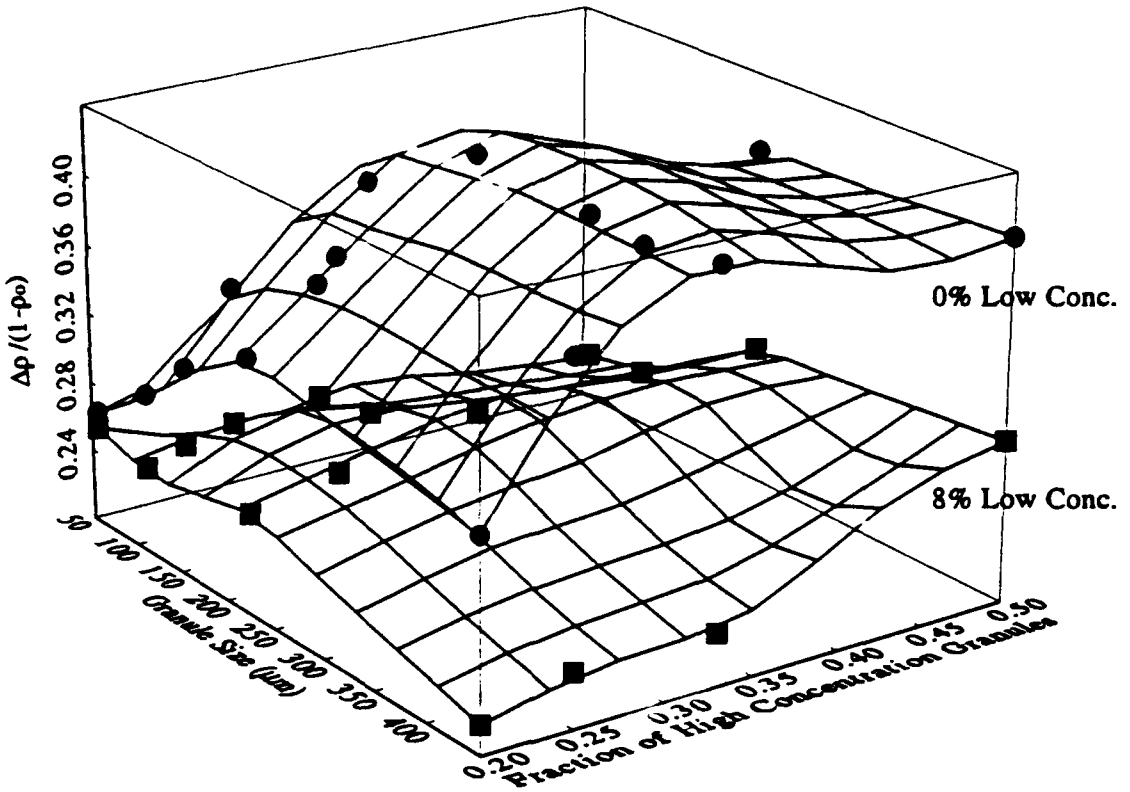

Figure 24 *Surface plot of the normalized matrix densification versus both the average granule size and the volume fraction of high concentration granules for the 0 and 8 vol% SiC low concentration granule compositions.*

inclusion. This increases the effective volume fraction of the inclusions, f_{eff}, according to

$$f_{eff} = f\left(1 + \frac{t}{r}\right)^3 \qquad 5$$

where f is the volume fraction of inclusions, t is the thickness of the layer of matrix particles, and r is the radius of the inclusions. For the 0.68 μm alumina and 4 μm SiC particles used here, a single layer of matrix particles adhering to the inclusions would increase f_{eff} to 2.4 f.

In homogeneous compacts the inclusions are relatively uniformly distributed so the effective volume fraction of inclusions would be $\approx$29 vol% which should strongly impede densification. A heterogeneous composite contains regions of both high and low inclusion concentration that will densify at different rates. The effective volume fraction of inclusions in the low concentration regions will be low enough so that these regions can densify more than the homogeneous compacts as shown in Figure 20, particularly when there are no inclusions in the low concentration regions. However, the regions containing high concentrations of inclusions densify nearly as well as the homogeneous compacts. The net effect is that the heterogeneous composites densify better than homogeneous compacts.

This explains why the composites made using low concentration granules containing 0 vol% SiC densify better than the other composites and the homogeneous compacts. However, it does not

directly explain the better densification of composites made using moderate fractions of large, high concentration granules. At moderate volume fractions of the high concentration granules the SiC is not so concentrated that these granules become rigid. As a result these moderate concentration granules can be "hot pressed" by the stresses developed during densification of the low concentration regions. However, this does not occur when the concentration of SiC particles in the high concentration granules is high since these regions are difficult to deform or when the concentration of SiC in the low concentration granules increases because the stresses necessary for "hot pressing" are not developed because of their weaker densification.

The effect of granule size on densification was shown in Figure 22 where it is seen that densification is impeded more for smaller granule sizes in the composites made from pure low concentration granules. This can be explained in two different ways. The first is that the composites made from smaller granules are more homogeneous than those made from the larger granules and therefore densify like the more homogeneous samples. The second is that the effective volume fraction of the high concentration granules will be higher than the actual volume fraction due to local constraint of the matrix as occurs around the individual inclusion particles. As the granule size increases, this effect disappears just as it does when the inclusion particles become large. The observed effect of granule size is felt to be a result of a combination of these two effects, especially since it occurs primarily for the composites made from purer low concentration granules.

3.2.4 Conclusions

The densification behavior of clustered Al_2O_3/SiC composites containing an average of 12 vol% SiC has been determined. It was found that moderately heterogeneous composites densified better than those that were either very homogeneous or very heterogeneous. The primary exception to the moderately heterogeneous rule was that those composites with the largest difference in SiC inclusion concentration between low concentration and high concentration regions densified better than those that were more homogeneous. We feel that this is because the purer low concentration granules densify so well that they "hot press" the granules containing moderate SiC concentrations.

4 Green Processing of ZrO_2/Al_2O_3 Composites

This aspect of the project focussed on developing an Al_2O_3/ZrO_2 composite system to investigate the effect of inclusion clustering. There should be little or no reaction between the constituents under the planned sintering conditions of 1400 to 1500°C for 1 to 4 hours. The elimination of matrix/inclusion reactions will make the effects of clustering easier to ascertain.

4.1 Slip Stabilization at High pH

The stability of Al_2O_3/ZrO_2 slips was investigated at high pH to determine the optimal conditions for fabrication of the Al_2O_3/ZrO_2 composite granules of different compositions. These granules would then be combined to create compacts with controlled inclusion inhomogeneity. Electrostatic stabilization at a solution pH of 12.4 (slip pH of 11.5 - 12.0) using Ammonia hydroxide (NH_4OH) was chosen based upon extensive low technology studies of the colloidal behavior of the Al_2O_3 and ZrO_2 powders. This pH was chosen based upon the results of many sedimentation experiments using varying volume fractions (2-40 vol%) of Al_2O_3 (Sumitomo AKP-15, nominal 0.68 μm particle size) and ZrO_2 (Magnesium Elektron E20, nominal particle size of 5 μm) separately in NH_4OH solutions ranging in pH from 8.0 to 13.5.

The results of the sedimentation experiments are shown in Figure 25 where it is seen that low to moderate solids loading slips of both powders exhibit minimal sedimentation rates over the entire pH range. However, the 20 vol% ZrO_2 slips exhibit higher sedimentation rates at lower pH suggesting that higher pH is probably desirable.

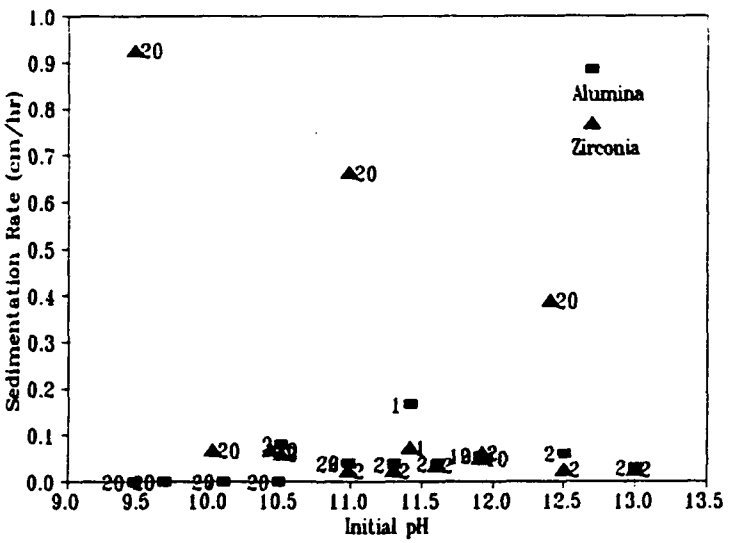

Figure 25 Sedimentation rates of the 0.68 μm Al_2O_3 and the 5 μm ZrO_2 powders. The internal labels are the volume percent of powder in the slip.

The change in the pH of the decantant was also measured after sedimentation to determine how much interaction there was between the powder and the NH_4OH solution. The results of these measurements are plotted in Figure 26 where it is seen that there are very large changes in pH at

lower initial values of the pH. A working pH of 12.4 was chosen because the individual sedimentation rates of the alumina and zirconia are both low and only small changes in pH occur in this region. This makes the slip system more robust with respect to small changes in the solution pH, powder surface chemistry, or other uncontrolled variables.

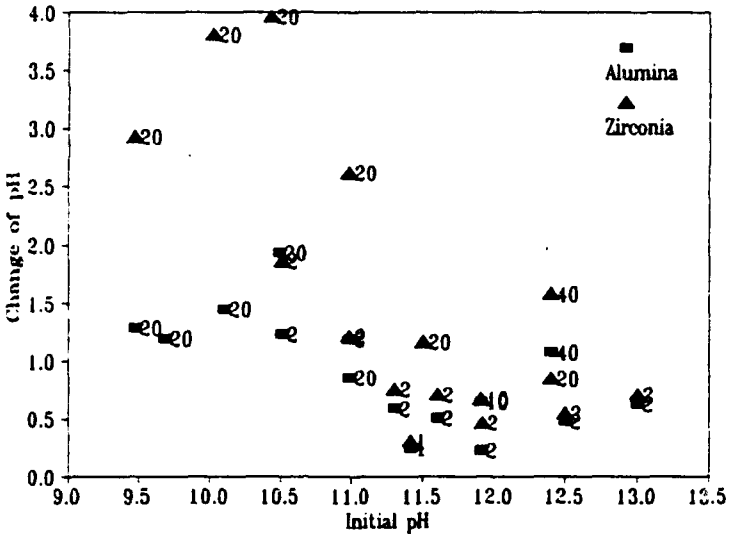

Figure 26 Change in pH for the 0.68 μm Al_2O_3 and 5 μm ZrO_2 powders during sedimentation. The internal labels refer to the volume percent of solids in the slips.

Several composites were fabricated from the alumina and zirconia at an initial slip pH of 12.4. These composites were sintered at 1400°C for four hours in air. Both the green and sintered densities of the composites were relatively low and quite variable. Therefore, this green processing route was abandoned.

4.2 Slip Coagulation at Low pH

Coagulation of the Al_2O_3/ZrO_2 slips at low pH was investigated since the the alumina and zirconia appeared to phase separate at high pH in some cases. Dispersing the powders in a suspension results in the development of strongly repulsive surface forces that prevent the particles from getting close enough together to be in the primary energy minima where Van der Waals forces cause floculation. The addition of a salt to an otherwise well dispersed suspension increases the ionic strength of the fluid. At an appropriate ionic strength, a weaker secondary energy minima is created at a larger interparticle separation than the primary minima. The particles in such a coagulated slip are then weakly bonded together which prevents sedimentation and other forms of segregation which are frequently detrimental to the properties of composites.

4.2.1 Experimental Procedure

Composites were fabricated from fine grained alumina (AKP-15, Sumitomo Chemical Co.) which is nominally 0.68 μm in diameter and zirconia (E-20, Magnesium Elektron, Inc.) which is

nominally 5 μm in diameter. The green processing methods employed have followed the previous works of F.F. Lange *et. al.*[21, 22] to produce a uniformly distributed and electrochemically stable slip. Both alumina and zirconia are well dispersed at a pH ranging from 2 to 3.5.[22] A mixture of the powders is initially dispersed in a pH 3 aqueous solution (HNO_3) at a solids loading of 33 vol%. These suspensions were ultrasonicated (VC600, Sonics and Materials, Inc.) at 100 W using a 50% cycle time for two minutes to break up agglomerates. The solution pH was then adjusted by addition of HNO_3 to maintain a pH of 3.

The slips were coagulated by adding a coagulating salt to increase the viscosity and prevent the larger, more massive zirconia particles from settling out through natural sedimentation. The coagulating salts and concentrations used in this study are listed in Table XI. In addition, it is felt that the coagulating salt creates a weak bond between the alumina particles and the zirconia that effectively coats the zirconia with alumina.[21] When combined with the impeded sedimentation this will dramatically improve the homogeneity of the zirconia distribution in the composites. The ammonium salts did not affect the pH of the suspension while the aluminum salts made the suspensions much more acidic. This effect was not compensated for and may have resulted in less than optimal slip properties.

Table XI Coagulating Salts and Concentrations

Salt	Molarity	Slip pH
NH_4Cl	1.8	3.0
NH_4NO_3	1.8	3.0
$Al(NO_3)_3$	1.8	1.41
$AlCl_3$	1.8	0.98
$AlCl_3$	0.9	0.43

The coagulated slips were then vacuum filtered to produce compacts. This was accomplished pouring the slip into ring mold (a 35 mm film can with the bottom removed) on a piece of filter paper in a glass fritted buchner funnel. The bottom of the buchner funnel was subjected to a vacuum of approximately 75 kPa while the slip was exposed to the atmosphere. The compacts were dried in air to constant weight followed by measurement of the green density based upon the mass and dimensions of the compacts. Some of the dry green compacts were crushed and sieved through a 150 μm sieve followed by isostatic pressing into pellets at 31 MPa. The compacts were sintered in air at 1400 to 1550°C with a four-hour isothermal hold and 5°C/minute heating and cooling rates. Sintered densities were measured using Archimedes' method. Selected specimens were mounted and polished followed by microstructural examination via SEM.

4.2.2 Results and Discussion

The fractional green density of the vacuum filtered composites made using 1.8 M NH_3Cl ranged from 0.50 to 0.59 as shown in Figure 27. The composites had a slightly higher density than either the pure alumina or zirconia, particularly for the samples that were subsequently sintered at 1450°C since they were made later than those fired at 1500°C when the process had been improved. This effect was seen with the other coagulants as well and is probably due to due to

the finer alumina particles filling the interstices between the coarser zirconia particles. These green densities are slightly lower than those reported by other investigators.[21, 23, 24]

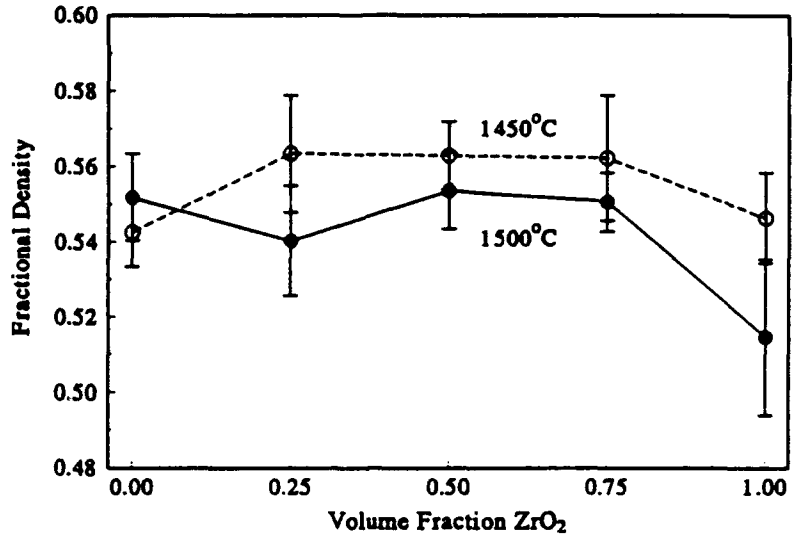

Figure 27 Green density of the Al_2O_3/ZrO_2 composites made using 1.8M NH_3Cl as a coagulant.

The fractional sintered densities for these composites are shown in Figure 28. The samples sintered at 1500°C reached a higher density than those sintered at 1450°C as expected although their green density was lower. The sintered density also decreases as the volume fraction of ZrO_2 is increased. However, it is better described by a weighted average of the densification behavior of the end members rather than the rapid decrease that is observed for sintering of systems containing hard, inert inclusions. The samples sintered at 1450°C are much more consistent than those sintered at 1500°C which is a consequence of improved green processing. This was confirmed upon examination of fracture surfaces where more large pores (100-500 μm) due to trapped air during vacuum filtration were seen in the 1500°C samples.

The effect of using different coagulating salts for the vacuum filtered composites is shown in Figure 29. The use of 1.8 M $AlCl_3$ increases the green density compared to the other salts. The composites coagulated using $AlCl_3$ have slightly higher sintered densities than the NH_3Cl coagulated composites which is felt to be a consequence of decomposition of $AlCl_3$ to form Al_2O_3. The composites coagulated using the nitrate salts densified the best which is probably a result of the elimination of the chlorine from the system which has been shown to impede densification of Al_2O_3. However, this data is too scattered to draw definitive conclusions about how these salts affect densification of these composites.

Crushing and pressing the composites removes the large pores formed during vacuum filtration and improves both the magnitude and the reproducibility of the densities as shown in Figure 30. The average fractional green densities are increased by ≈ 0.085 when the compacts are crushed and pressed while the fractional sintered densities are increased by ≈ 0.055. An interesting point is that the highest sintered density was obtained using 0.9M $AlCl_3$ while the lowest sintered density resulted from use of 1.8M $AlCl_3$.

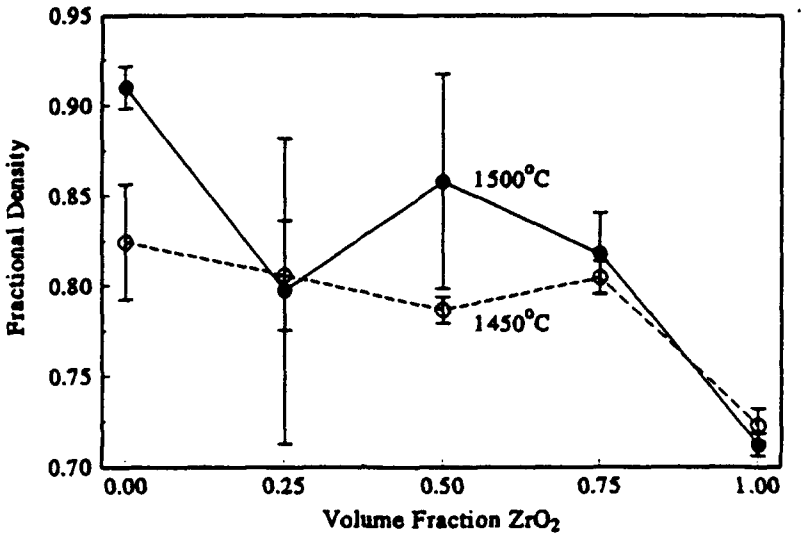

Figure 28 Fractional sintered densities versus volume fraction of ZrO_2 for the composites coagulated with 1.8 M NH_3Cl.

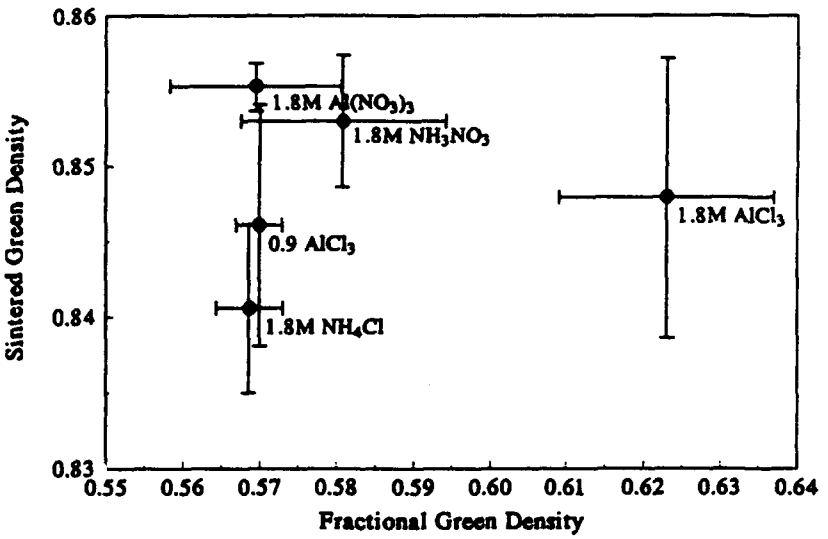

Figure 29 Sintered density versus green density for 75 vol% ZrO_2 vacuum filtered composites coagulated with different salts and sintered at 1450°C.

Examination of fracture surfaces of the green compacts showed that there were many voids due to trapped air within the compacts. These voids were between 100 and 500 μm in diameter and much too large to close during sintering. SEM examination of the crushed and pressed pellets revealed that the primary voids present were in the 2-5 μm range. Some of these pellets did exhibit long (10-50 μm) crack like voids. It is assumed that these are caused by stress relaxation of over pressurization during compaction.

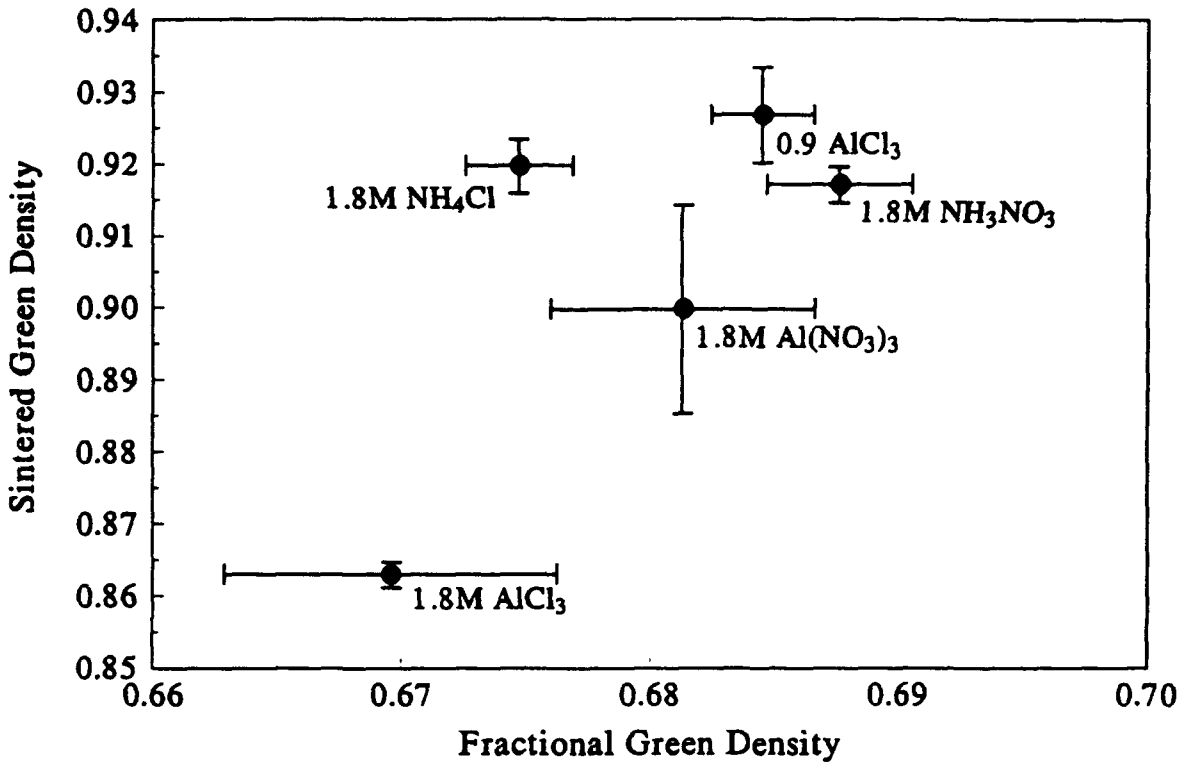

Figure 30 Sintered density versus green density for 75 vol% ZrO_2 crushed and pressed composites coagulated with different salts and sintered at 1450°C.

4.2.3 Conclusions

None of the salts investigated here (NH_4Cl, NH_4NO_3, $AlCl_3$, $Al(NO_3)_3$) appear to be clearly superior to the others. All of the salts resulted in composites in which the alumina and zirconia were reasonably well distributed. NH_4Cl is suitable for use based upon these results and those of Lange *et. al.*[23] The use of NH_4NO_3 is promising since it resulted in slightly higher green and sintered densities than NH_4Cl. The aluminum salts also show promise since they should leave Al_2O_3 when they decompose upon heating. However, the addition of both $AlCl_3$ and $Al(NO_3)_3$ dramatically reduced the pH of the slip which may have caused problems during consolidation since the interparticle attractions become strongly attractive at very low pH for both alumina and zirconia.

Vacuum filtration resulted in large pores due to air bubbles in these Al_2O_3/ZrO_2 composites. Crushing and isopressing the resulting granules improved both the green and sintered densities, but the sintered densities were not high enough for most applications under the sintering conditions studied here. We would like to suggest that further studies by carried out using either slip casting or pressure filtration of carefully de-aired coagulated slips to eliminate the formation of these large pores.

5 Experimental Design

We have conducted extensive studies to find the optimal experimental scheme for studying the complicated combination of variables involved in this project. This study of inclusion clustering examines the effect of overall ZrO_2 inclusion volume fraction, the spatial extent of clustering, the degree of inhomogeneity between high and low volume fraction granules, and the relative abundance high to low volume fraction regions. This results in a total of five different variables: the size of the granules that are used to create the composites, and the four interrelated compositional variables that are the bulk concentration of zirconia, the fraction of zirconia in the low concentration granules, the fraction of the inclusion granules, and the fraction of zirconia in the high concentration granules. The last four variables are related by the equation

$$f_{ZrO_2,bulk} = F_{incl} f_{ZrO_2,incl} + (1 - F_{incl}) f_{ZrO_2,mat} \qquad 6$$

where $f_{ZrO_2,bulk}$ is the bulk volume fraction of ZrO_2 in the composite, F_{incl} is the volume fraction of high concentration granules, $f_{ZrO_2,incl}$ is the volume fraction of ZrO_2 in the high concentration granules, and $f_{ZrO_2,mat}$ is the volume fraction of ZrO_2 in the low concentration granules so that only three of the variables are independent.

Several different experimental approaches were researched and considered to carry out this study. We were particularly interested in obtaining results that will produce data that will fully represent a response surface showing how changes in two of the five variables affect composite densification. A full factorial experimental approach was eliminated since it would require too many experiments. Therefore, a partial factorial experimental approach was selected. Unfortunately, none of the standard partial factorial experimental approaches such as Taguchi, Box-Hunter, or traditional response surfaces were applicable to this system since they did not cover the parameter space well enough or were not amenable to the constraints imposed by Equation 6.

We have designed a partial factorial experiment that allows a full quartic response surface to be fit to any two of the parameters while two of the parameters are held constant and the final parameter is varied according to equation 6. This experimental design can be envisioned as a series of two-dimensional slices through the four-dimensional parameter space defined by equation 6 with the granule size being a separate parameter. The number of different slices is listed for each combination of variable and constant parameters in Table X. This experimental design uses a total of approximately 120 different composites out of the over 1000 different composites that would be required in a full factorial experiment giving the same coverage of the parameters.

Table X Experimental Design Summary for the Clustering Project

Constant Parameter	Variable Parameters	Number of Slices
$f_{ZrO_2,\,bulk}$	$f_{ZrO_2,\,mat}$ and $f_{ZrO_2,\,incl}$	4 @ 0.08, 0.16, 0.24, & 0.32
F_{incl}	$f_{ZrO_2,\,bulk}$ and $f_{ZrO_2,\,mat}$	4 @ 0.2, 0.4, 0.6, & 0.8
$f_{ZrO_2,\,incl}$	$f_{ZrO_2,\,bulk}$ and $f_{ZrO_2,\,mat}$	4 @ 0.2, 0.4, 0.6, & 0.8
$f_{ZrO_2,\,mat}$	$f_{ZrO_2,\,bulk}$ and $f_{ZrO_2,\,incl}$	5 @ 0, 0.04, 0.08, 0.12, & 0.16

The complex experiment described above was not conducted due to a change of personnel and the change of the green processing from conventional high pH colloidal routes to coagulation at low pH. We planned to fabricate approximately five pellets of each composition described above. These would be made in four or five different granule sizes and sintered at two different temperatures. The Al_2O_3/ZrO_2 composite granules need to be as homogeneous as possible to insure that most of the inhomogeneity in the compacts due to the experimental parameters and not inhomogeneities during slip casting. These composites were to be pressureless sintered at 1400 to 1600°C for 1 to 4 hrs along with control composites made from a single type of granule. The exact sintering schedule will be chosen so that the composites that contain a low volume fraction of ZrO_2 reach fractional densities of 0.90 to 0.96 while those that contain higher volume fractions do not densify as well. A preliminary study using the as cast Al_2O_3/ZrO_2 composites was conducted and reported on earlier to determine the optimal sintering time and temperature.

The densification and microstructure of this series of over 100 composites were to be evaluated. Two-dimensional slices from the four-dimensional response surface of the densification will be plotted to examine how the various types of inhomogeneity affect the densification. This information will be combined with the microstructural evaluation to determine which of the currently available models of densification of composites best describes the behavior and how it can be improved to better describe the behavior of these very inhomogeneous materials. The fracture toughness of some composites will be measured via the indentation technique since there is recent work that suggests that clustering the ZrO_2 particles results in higher toughness Al_2O_3/ZrO_2 composites than completely homogeneous materials.[19] If this is the case for our materials and the improved densification of somewhat inhomogeneous Al_2O_3/SiC composites continues, it may be possible to develop high toughness materials that are particularly easy to fabricate.

6 Drying of Composites

Many researchers are currently investigating the green processing of ceramics to improve the final properties. Slip casting of well dispersed slips containing the ceramic powder(s) of interest is a very promising technique. Several investigations are ongoing at various institutions to determine how different ceramic powders may be optimally co-dispersed to create composite green bodies. However, relatively little effort has focussed on the drying of these composite green bodies.

The presence of inclusions that are larger than the matrix particle size can result in the formation of a stiff network that cannot be deformed to accommodate the shrinkage of the matrix. These large inclusions include agglomerates and reinforcing particles, fibers, and whiskers. This will result in the formation of flaws in the matrix particle packing which will be difficult to eliminate during sintering. The effects of such a network are seen most frequently when the percolation limit for inclusion contact is exceeded. For a random distribution of spherical particles the percolation limit is approximately 16 volume percent inclusions. The percolation limit for inclusions of other morphologies is lower than 16 vol% and drops dramatically for high aspect ratio fibers or whiskers.

Composites composed of fine Al_2O_3 powder (AKP-15, 30, and 50 supplied by Sumitomo Chemical Co.) which contained various volume fractions of larger, roughly equiaxed SiC (≈ 10 μm diameter supplied by Norton Co. and air classified in a previous study[15]) or ZrO_2 (E30, SC30, and SC101 supplied by Magnesium Elektron and DK-2 supplied by Zirconia Sales (America) Inc.) inclusions were fabricated by slip casting. Slips contained 0 to 60 vol% inclusions and were dispersed using Na-PAA (Daxad 30 supplied by W.R. Grace & Co.) for the SiC inclusions and Na-PMAA (37LN10-35 supplied by W.R. Grace & Co.) for the ZrO_2 inclusions. The slips were then ultrasonically disrupted or vibratory milled for 10 minutes to obtain homogeneous slips of near minimal water content. These slips were then cast on the surface of a dampened plaster bat in cylindrical plastic molds that were either 12 or 30 mm in diameter. The pellets were dried on the plaster for ≈ 24 hours followed by ≈ 24 hours at 85°C to remove the remaining water. After cooling to room temperature, the density of each pellet was determined from measurement of the mass, diameter, and length of the pellet.

For all of the composites studied here it was found that the density changed behavior as a function of inclusion volume fraction at 22 to 30 vol% inclusions as shown in Figure 31 for the 10 μm SiC inclusions in AKP-15 Al_2O_3. The density of the compact is limited by the packing of the matrix particles for inclusion concentrations between 0 and 26 vol% as shown by the constant matrix density in this range. For higher inclusion concentrations the density is limited by the packing of the inclusion particles as is seen by the constant bulk density for these composites. This change of behavior is attributed to the formation of a percolation network by the inclusions that impedes further shrinkage. This effective percolation limit is higher than the predicted theoretical percolation limit based upon inclusion morphology (≈ 12 to 16 vol%).

The effective percolation limit was also found to depend upon both the inclusion size and the matrix particle size. Figure 32 shows that decreasing the matrix particle size from 0.68 to 0.39 μm with 5 μm ZrO_2 inclusions lowers the effective percolation limit from 0.28 to 0.22. Figure 33 shows that increasing the inclusion size from 5 to 14 μm in a 0.39 μm Al_2O_3 matrix increases the effective percolation limit from 0.22 to 0.26. The effective percolation limit

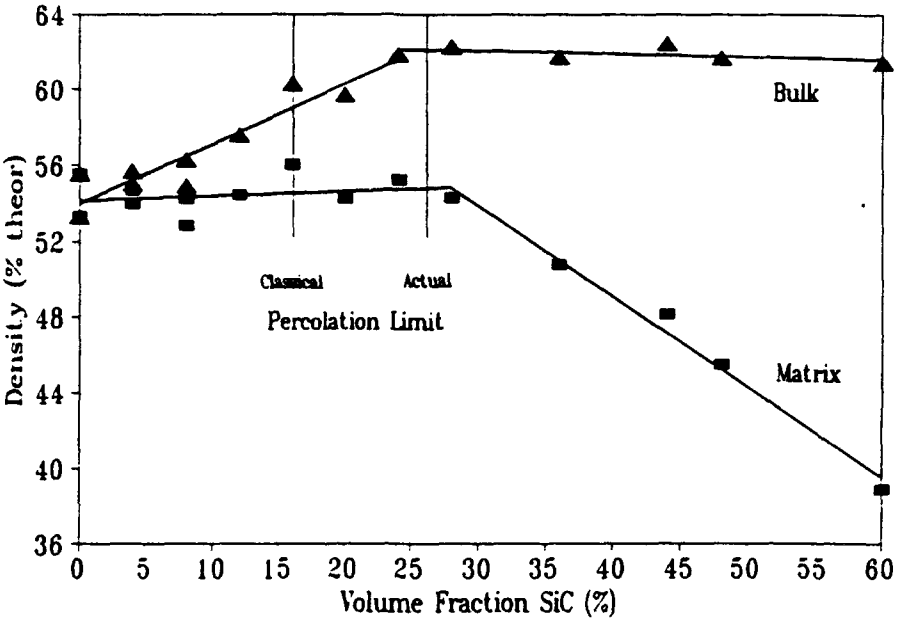

Figure 31 The bulk and matrix fractional densities for composites composed of 10 μm SiC in a 0.68 μm Al_2O_3 matrix showing both the predicted and actual percolation limits.

increases as both the matrix particle and inclusion size increase. These findings are consistent with the percolation network being collapsed by the capillary forces during drying.

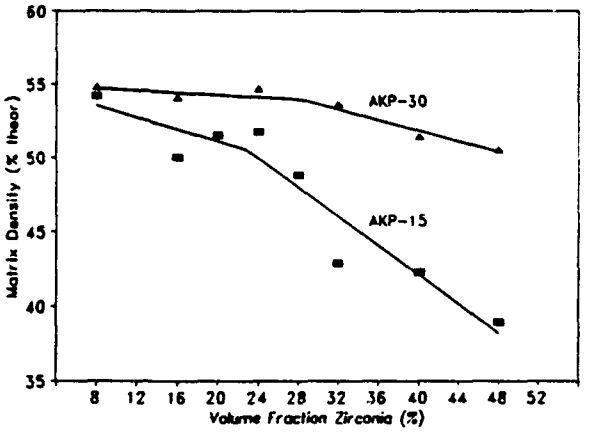

Figure 32 Matrix green density for Al_2O_3/ZrO_2 composites made using 5 μm ZrO_2.

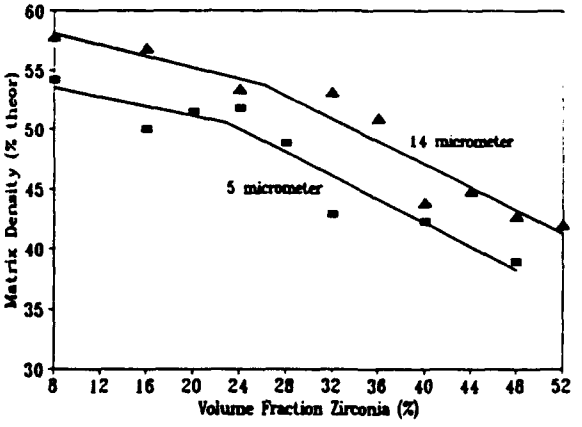

Figure 33 Matrix green density for Al_2O_3/ZrO_2 composites made with AKP-15 Al_2O_3.

This work was published as "Effective Percolation Limit in the Drying of Ceramic Composites", M.W. Weiser and K.C. Key, pp. 95-100 in Ceramic Trans. Vol. 26: Forming Science and Technology for Ceramics, ed. by M.J. Cima, American Ceramic Society, Columbus, OH 1992

7 Fabrication of Toughened Ferrites

The fabrication of toughened ferrites was incorporated into this project because this composite system densifies better than any other standard crystalline ceramic composite system. In addition, great progress was being made, and the primary source of funding had temporarily been discontinued and I did not desire to stop supporting the student. This project has improved the toughness of a Mn-Zn ferrite from 0.9 MPa$\sqrt{m}$ to nearly 3 MPa$\sqrt{m}$ by making ferrite/ZrO_2. During the first phase of the project we were attempting to maximize the toughness so the microstructure was not optimized for the magnetic properties.

Composites composed of a fine grained Mn-Zn ferrite (RH-52B Ampex Corp. $\approx$1-3 μm particles) and a up to 30 vol% of either ZrO_2 powder (Zircar ZYP-4.5, Tosoh USA TZ-0 and TZ-3Y, or Zirconia Sales DK-2) or ZrO_2 fibers (Zircar ZYBF-2) were fabricated by slip casting and pressureless sintering. Upon firing at 1400 to 1500°C for 1 to 4 hours it was found that the composites densified extremely well reaching densities over 90 % theoretical. The results for the Zircar zirconia materials are shown in Figure 34 where it is seen that most of the composites densified better than the pure matrix material. This is in direct contradiction to the observed behavior of most crystalline matrix ceramic composites. We feel that there may be several contributions to the very good densification of the composites in this system. These contributions include but are not limited to control of the ferrite grain growth by the inclusions and/or the ferrite powder coating the ZrO_2 inclusions to prevent the formation of percolation networks. The fibers used in this study were approximately 8 by 500 μm and intended for furnace insulation rather than ceramic reinforcement.

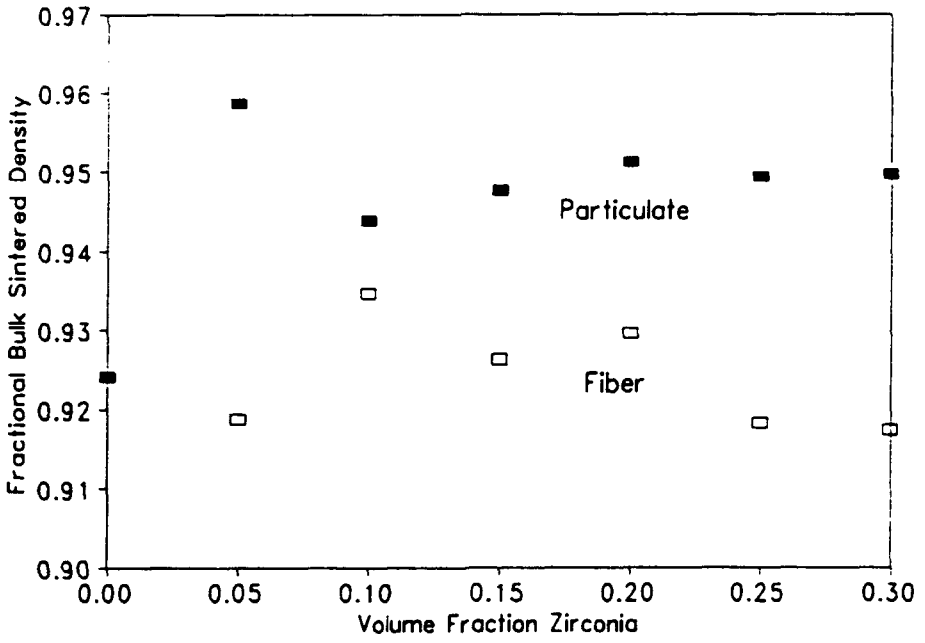

Figure 34 The density of ferrite/ZrO_2 composites containing various volume fractions of either ZrO_2 particulate or fibers after sintering for 1 hour at 1450°C.

The fracture toughness of most of the composites was significantly higher than that of the pure ferrite. The peak fracture toughness was 2.84 MPa$\sqrt{m}$ as determined by vickers indentation for

the composite that contained 25 vol% TZP (4.5 mol% Y_2O_3) as shown in Figure 35. Unfortunately, the composites with the best fracture toughness exhibited very poor magnetic properties with typical values of approximately 10% of that of the pure ferrite. We have attempted to distribute the ZrO_2 particles non-uniformly to improve the permeability while maintaining the high fracture toughness based upon the results of Wang and Stevens with Al_2O_3/ZrO_2 composites.[19] However, sintering damage developed which limited the fracture toughness.

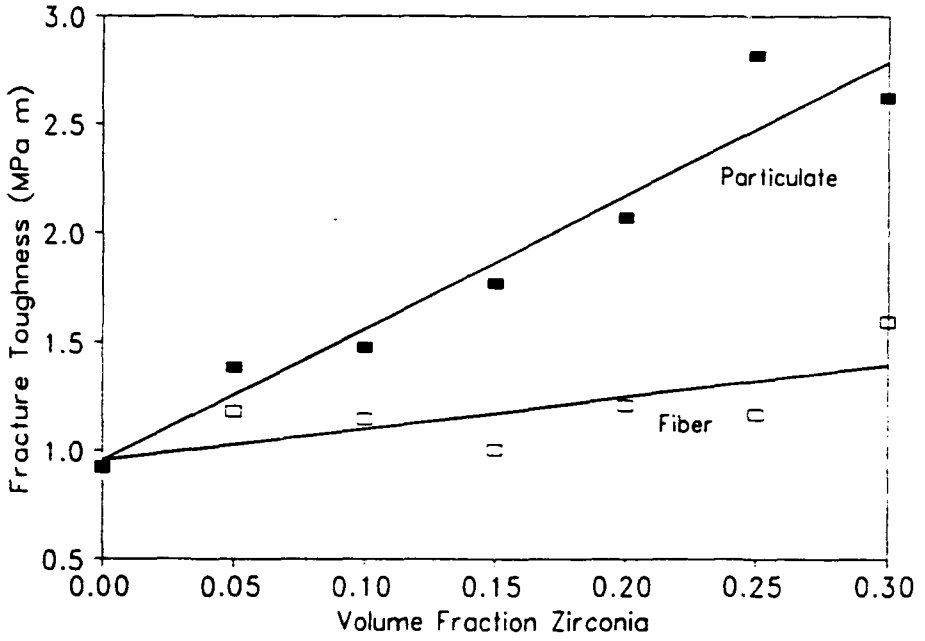

Figure 35 Fracture toughness (MPa$\sqrt{m}$) of Mn-Zn ferrites reinforced with either 5 μm partially stabilized ZrO_2 or fully stabilized ZrO_2 insulation fiber.

These results have been presented at the 93rd Annual Meeting of the American Ceramic Society and we are in the process of preparing a paper on these preliminary results.

8 Transient Liquid Phase Sintering

Transient liquid phase sintering is being investigated as a possible method to improve the densification of ceramic matrix composites. This is based upon the great success seen in monolithic materials and the limited success seen in Al_2O_3/SiC_w composites at very high temperature by the Oak Ridge group. In addition, the initial funding for this project ran out before it was completed and I felt that transferring the study to this project would encourage the minority undergraduate student involved to continue his studies and give me a very capable lab assistant over the next couple of years.

We used LiF fluxed $BaTiO_3$ (Tricon P supplied by TAM Ceramics) with either large SiC or $BaTiO_3$ inclusions to model the densification of transient liquid phase sintered composites. The initial results with the SiC inclusions suggest that the inclusions impede densification much more than in most ceramic composites. This is probably a result of the very transient nature of the liquid that can densify the monolithic material but does not have enough time to densify the composite. There are indications that the SiC particulate reacts with either the $BaTiO_3$ or the LiF based liquid at the sintering temperatures of 850 to 1050°C although SiC is considered to be relatively corrosion resistant at this temperature.

To eliminate problems with SiC reaction we produced inclusions composed of LiF fluxed $BaTiO_3$ with the same composition as the matrix and the same size as the SiC inclusions. This eliminates the possibility of reactions, does not cause too many problems with abnormal grain growth since the sintering program is both short and at relatively low temperatures, and allow us to clearly determine the densification behavior. The use of highly fluxed $BaTiO_3$ ($\approx$20 to 50 vol% LiF) particles were considered as the flux in the system so that the liquid is not as transient. Combining the LiF with part of the matrix should create a less reactive liquid that is not absorbed by the remaining $BaTiO_3$ powder as quickly. Unfortunately, the student involved in this project left the project soon after this phase was started so there are no results to report.

9 Publications

9.1 In Print

1 "Effective Percolation Limit in the Drying of Ceramic Composites", M.W. Weiser and K.C. Key, pp. 95-100 in Ceramic Trans. Vol. 26: Forming Science and Technology for Ceramics, ed. by M.J. Cima, American Ceramic Society, Columbus, OH 1992

9.2 Anticipated

"Toughening of Mn-Zn Ferrites", M.W. Weiser, T.J. Garino, and W.J. Mangan

"Densification of Inhomogeneous Ceramic Composites: Clustered Al_2O_3/SiC", M.W. Weiser, D.J. Frew, W.D. Willis, and T.J. Garino

"Densification of Coagulated Al_2O_3/ZrO_2 Composites", J.L. Roberts and M.W. Weiser

"Fiber Aspect Ratio Effects in Ceramic Matrix Composites: I, Fractionation and Green Processing", P.G. Madrid and M.W. Weiser

"Fiber Aspect Ratio Effects in Ceramic Matrix Composites: II, Sintering and Densification", P.G. Madrid, M.W. Weiser, and K. Ewsuk

"Fiber Aspect Ratio Effects in Ceramic Matrix Composites: III, Indentation Fracture Toughness", M.W. Weiser and P. Rodriguez

10 Presentations

The American Ceramic Society, 93rd Annual Meeting, April 1991, Cincinnati, OH
- "Effective Percolation Limit in the Drying of Ceramic Composites", M.W. Weiser and K.C. Key
- "Zirconia Toughened Ferrites: I, Mechanical Properties", M.W. Weiser, W.J. Mangan, and T.J. Garino
- "Zirconia Toughened Ferrites: II, Magnetic Properties", T.J. Garino, M. Harrington, M.W. Weiser, W.J. Mangan

Ceramics and Advanced Materials Symposium, October 1990, Santa Fe, NM
- "Densification of Al_2O_3 Matrix Composites with Controlled SiC Inclusion Distributions", M.W. Weiser, D. Frew, W.D. Willis, and T.J. Garino
- "Transient Liquid Phase Sintering of Composites", R. Rubio and M.W. Weiser

Ceramics and Advanced Materials Symposium, Albuquerque, NM, October 24-25, 1991
- "Densification of Ceramic Composites: Preliminary Whisker Length Effects, P.G. Madrid and M.W. Weiser

Wright-Patterson Air Force Base, Dayton OH, July 1991
"Pressureless Sintering of Ceramic Composites", M.W. Weiser

Symposium on Ceramics and Advanced Materials, Albuquerque, NM, October 25-26, 1993
"Densification of Ceramic Composites: Short Fiber Length Effects", P.G. Madrid and M.W. Weiser

AFOSR Ceramics and Glass Contractor's Meeting, Washington, DC, October 26-29, 1992
"Pressureless Sintering of Ceramic Matrix Composites", M.W. Weiser, P.G. Madrid, J.L. Roberts, and C.F. Lampiris

Ceramics and Advanced Materials Symposium, Santa Fe, NM, October 23, 1992
"Sintering of Al_2O_3 and Al_2O_3/ZrO_2 Compacts Slip Cast from Coagulated Slips", J.L. Roberts, M.W. Weiser, and C.F. Lampiris

Ceramics and Advanced Materials Symposium, Albuquerque, NM, October 24-25, 1991
"Densification of Ceramic Composites: Preliminary Whisker Length Effects", P.G. Madrid and M.W. Weiser

11 Students Affiliated with the Project

11.1 Graduate Students Supported

1 Jay Pape, 1/90 - 8/90, "Initiation of the Inclusion Aspect Ratio Study", Jay left the project to take a position with DOE Albuquerque

2 Philip Madrid, 8/90 - 12/92, "Effect of Inclusion Aspect Ratio on Composite Densification", Phillip is splitting his time during the academic year between teaching and research

3 Keith B. Fong, 3/91, "Microscopy Support", Keith is completing a separate project examining the drying of powder compacts

4 John L. Roberts, 8/92 - 3/93, "Sintering of Inhomogeneous Composites"

11.2 Undergraduate Students Supported

1 Kami C. Key, 1/91 - 5/91, "Effective Percolation Limit in the Drying of Composites", Kami graduated and took a position with the Naval Air Development Center.

2 Roger Rubio, 11/90 - 9/91, "Transient Liquid Phase Sintering of Composites", Roger has just completed hi Freshman year at UNM after working with me as a High School senior.

3 William J. Mangan, 1/91 - 5/91, "Densification of Composite Ferrites", Bill completed his BSME about a year ago and is currently working on an MBA while continuing his running career and working part-time on this project to keep himself involved in science.

4 Chris Lampiris, 5/91 - 12/91, "Effect of Inclusion Distribution on Densification of Ceramic Composites", Chris intends to continue this work into a Master's Thesis after he receives his BS in 12/91

5 Danny J. Frew, 4/1/91 - 5/15/91, "Densification of Al_2O_3 Matrix Composites with Controlled SiC Inclusion Distributions", Danny completed most of the experimental aspects of this study and began graduate study with a colleague in fracture mechanics.

11.3 Graduate Independent Study Students

1 Patrick J. Rodriguez, "Fracture Toughness of Short Fiber Ceramic Matrix Composites", MS Project, 8/23/93 - Present, MS ME is expected in December 1994

11.4 Undergraduate Independent Study Students

1 Victor Maestos, "Toughening of Magnetic Ferrites", ME Junior, 5/24/91 - 12/15/92

12 References

1 D. Bradley, The Hydrocyclone, *Volume 4 of International Series of Monographs in Chemical Engineering*, ed. by P.V. Danckwerts, Pergamon Press, Oxford, 1965

2 K.L. Luthra, "Chemical Interactions in High-Temperature Ceramic Composites", *J. Am. Ceram. Soc.*, **71** [12] 1114-20 (1988)

3 K.B Fong, "Optimizing Slip Cast Alumina Powder Compact Drying and Microstructure Using Taguchi Method Design of Experiments", Masters Thesis, University of New Mexico, Albuquerque, New Mexico, 1991

4 G. Pezzotti, I. Tanaka, T. Okamoto, M. Koizumi, and Y. Miyamoto, "Processing and Mechanical Properties of Dense Si_3N_4-SiC-Whisker Composites Without Sintering Aids", *J. Am. Ceram. Soc.*, **72** [8] 1461-64 (1989)

5 W.J. Tseng and P.D. Funkenbusch, "Microstructure and Densification of Pressureless-Sintered Al_2O_3/Si_3N_4-Whisker Composites", *J. Am. Ceram. Soc.*, **75** [5] 1171-75 (1992)

6 M.D. Sacks, H.W. Lee, and O.E. Rojas, "Suspension Processing of Al_2O_3/SiC Whisker Composites", *J. Am. Ceram. Soc.*, **71** [5] 370-379 (1988)

7 M.D. Sacks, H.W. Lee, and O.E. Rojas, "Pressureless Sintering of SiC Whisker-Reinforced Composites", *Ceram. Eng. Sci. Proc.*, **9** [7-8] 741-754 (1988)

8 T.N. Tiegs and D.M. Dillard, "Effect of Aspect Ratio and Liquid-Phase Content on Densification of Alumina-Silicon Carbide Whisker Composites", *J. Am. Ceram. Soc.*, **73** [5] 1440-42 (1990)

9 T.N. Tiegs and P.F. Becher, "Sintered Al_2O_3-SiC-Whisker Composites", *Am. Ceram. Soc. Bull.*, **66** [2] 339-42 (1987)

10 C.C. Furnas, "The Relations Between Specific Volume, Voids, and Size Composition in Systems of Broken Solids of Mixed Sizes", *US Bur. Mines Rep. Invest.*, **2894** (1928)

11 G.L. Messing and G.Y. Onoda, Jr., "Inhomogeneity-Packing Density Relations in Binary Powders-Experimental Studies", *J. Am. Ceram. Soc.*, **61** [7-8] 363-66 (1978)

12 E.A. Holm and M.J. Cima, "Two-Dimensional Percolation in Ceramic Matrix-Ceramic Whisker Composites", *J. Am. Ceram. Soc.*, **72** [2] 303- 305 (1989)

13 S.J. Barclay, J.R. Fox, and H.K. Bowen, "Processing of Pressureless-Sintered SiC Whisker-Reinforced Al_2O_3 Composites", *J. Mater. Sci.*, **22** 4403-06 (1987)

14 I. Balberg, "Recent Developments in Continuum Percolation", *Phil. Mag. B*, **56** [6] 991-1003 (1987)

15 M.W. Weiser and L.C. De Jonghe, "Inclusion Size and Sintering of Composite Powders", *J. Am. Ceram. Soc.*, **71** [3] C125-C127 (1988)

16 T. Kimura, H. Kajiyama, J. Kim, and T. Yamaguchi, "Effect of Inclusion Size on the Densification of ZnO-$Zn_7Sb_2O_{12}$", *J. Am. Ceram. Soc.*, **72** [1] 140-41 (1989)

17 J. Cesarano III and I.A. Aksay, "Processing of Highly Concentrated Aqueous α-Alumina Suspensions Stabilized with Polyelectrolytes", *J. Am. Ceram. Soc.*, **71** [12] 1062-67 (1988)

18 A.G. Evans, "Considerations of Inhomogeneity Effects in Sintering", *J. Am. Ceram. Soc.*, **65** [10] 497-501 (1982)

19 J. Wang and R. Stevens, "Review: Zirconia-Toughened Alumina (ZTA) Ceramics", *J. Mater. Sci.*, **24** 3421-40 (1989)

20 F.F. Lange, "Approach to Reliable Powder Processing", Vol 1, *Ceramic Powder Science IIB*. Edited by G.L. Messing, E.R Fuller, Jr., and H. Hausner. American Ceramic Society, Westerville, OH, 1988

21 B.V. Velamakanni, J.C. Chang, F.F. Lange, D.S. Pearson, "New Method for Efficient Colloidal Particle Packing via Modulation of Repulsive Lubricating Hydration Forces", *Langmuir*, **6** [7] 1323-5 (1990)

22 I.A. Aksay, F.F. Lange, B.I. Davis, "Uniformity of Al_2O_3- ZrO_2 Composites by Colloidal Filtration", *Am. Ceram. Soc.*, **66** [10] C-190-2

23 J.C. Chang, D.V. Velamakanni, F.F. Lange, D.S. Pearson, "Centrifugal Consolidation of Al_2O_3 and Al_2O_3/ZrO_2 Composite Slurries vs Interparticle Potentials: Particle Packing and Mass Segregation", *J. Am. Ceram. Soc.*, **74** [9] 2201-4 (1991)

24 D.J. Green and M.G. Metcalf, "Properties of Slip-Cast Transformation-Toughened ß"-Al_2O_3/ZrO_2 Composites", *Bull. Am. Ceram. Soc.*, **63** [6] 803-20 (1984)

25 A. Bleier, "Models of the Oxide-Solution Interface", presented at the 94th Annual Meeting of the American Ceramic Society, Minneapolis, MN, April 15, 1992 (Paper No. 20-SIV92)

26 T. Garino, "Heterocoagulation as an Inclusion Coating Technique for Ceramic Processing", *J. Am. Ceram. Soc.*, **75** [3] 514-18 (1992)

13 Bibliography

27 G.L. Messing and G.Y. Onoda Jr., "Sintering of Inhomogeneous Binary Powder Mixtures", *J. Am. Ceram. Soc.*, **64** [8] 468-72 (1981)

28 J.P. Smith and G.L. Messing, "Sintering of Bimodally Distributed Alumina Powders", *J. Am. Ceram. Soc.*, **67** [4] 238-42 (1984)

29 R. Raj and R.K. Bordia, "Sintering Behavior of Bi-Modal Powder Compacts", *Acta Metall.*, **32** [7] 1003-19 (1984)

30 W.H. Tuan and R.J. Brook, "Sintering of Heterogeneous Ceramic Compacts: Part 2, ZrO_2-Al_2O_3", *J. Mater. Sci.*, **24** 1953-58 (1989)

31 B. Kellet and F.F. Lange, "Stresses Induced by Differential Sintering Powder Compacts", *J. Am. Ceram. Soc.*, **67** [5] 369-71 (1984)

32 F.F. Lange, T. Yamaguchi, B.I. Davis, and P.E.D. Morgan, "Effect of ZrO_2 Inclusion on the Sinterability of Al_2O_3", *J. Am. Ceram. Soc.*, **71** [6] 446-48 (1988)

33 F.F. Lange, "Densification of Powder Rings Constrained by Dense Cylindrical Cores", *Acta. Metall.*, **37** [2] 697-704 (1989)

34 H.M. Jang, W.E. Rhine, and H.K. Bowen, "Densification of Alumina-Silicon Carbide Powder Composites: II, Microstructural Evolution and Densification", *J. Am. Ceram. Soc.*, **72** [6] 954-58 (1989)

35 M.N. Rahaman, L.C. De Jonghe, and R.J. Brook, "Effect of Shear Stress on Sintering", *J. Am. Ceram. Soc.*, **69** [1] 53-58 (1986)

36 L.C. De Jonghe and M.N. Rahaman, "Sintering Stress of Homogeneous and Heterogeneous Powder Compacts", *Acta Metall.*, **36** [1] 223-229 (1988)

37 G.W. Scherer and S.M. Rekhson, "Viscoelastic-Elastic Composites: I, General Theory", *J. Am. Ceram. Soc.*, **65** [7] 352-60 (1982)

38 G.W. Scherer, "Sintering with Rigid Inclusions", *J. Am. Ceram. Soc.*, **70** [10] 719-25 (1987)

39 C-H. Hsueh, "Sintering of Whisker-Reinforced Ceramics and Glasses", *J. Am. Ceram. Soc.*, **71** [10] C442-C444 (1988)

40 C-H. Hsueh, A.G. Evans, and R.M. McMeeking, "Influence of Multiple Heterogeneities on Sintering Rates", *J. Am. Ceram. Soc.*, **69** [4] C64-C66 (1986)

41 L.C. De Jonghe, M.N. Rahaman, and C-H. Hsueh, "Transient Stresses in Bimodal Compacts During Sintering", *Acta Metall.*, **34** [7] 1467-71 (1986)

42 K.R. Venkatachari and R. Raj, "Shear Deformation and Densification of Powder Compacts", *J. Am. Ceram. Soc.*, **69** [6] 499-506 (1986)

43 R.K. Bordia and G.W. Scherer, "Overview No. 70, On Constrained Sintering - I. Constitutive Model for a Sintering Body", *Acta Metall.*, **36** [9] 2393-97 (1988)

44 R.K. Bordia and G.W. Scherer, "Overview No. 70, On Constrained Sintering - II. Comparison of Constitutive Models", *Acta Metall.*, **36** [9] 2398-2409 (1988)

45 R.K. Bordia and G.W. Scherer, "Overview No. 70, On Constrained Sintering - III. Rigid Inclusions", *Acta Metall.*, **36** [9] 2411-2416 (1988)

46 F.F. Lange, "Constrained Network Model for Predicting Densification Behavior of Composite Powders", *J. Mater. Sci.*, **2** [1] 15-65 (1987)

47 J. Boissonade, F. Barreau, and F. Carmona, "The Percolation of Fibres with Random Orientations: A Monte Carlo Simulation", *J. Phys. A*, **16** 2777-87 (1983)

48 S.T. Buljan, A.E. Pasto, H.J. Kim, "Ceramic Whisker and Particulate Composites: Properties, Reliability, and Applications", *Ceramic Bulletin*, **68** [2] 387-394 (1989)

49 V.J. Tennery, "Ceramics in Engines - An International Status Report", *Ceramic Bulletin*, **68** [2] 362-365 (1989)

50 J.J. Mecholsky, Jr., "Engineering Research Needs of Advanced Ceramics and Ceramic-Matrix Composites", *Ceramic Bulletin*, **68** [2] 367-375 (1989)

51 M.W. Lindley and D.J. Godfrey, "Silicon Nitride Ceramic Composites with High Toughness", *Nature*, **229** 192-3 (1971)

52 M.F. Ashby and D.R.H. Jones, "Engineering Materials 2", Pergamon Press, Oxford, England 1986

53 C.L. Fan and M.N. Rahaman, "Factors Controlling the Sintering of Ceramic Particulate Composites: I, Conventional Processing", *J. Am. Ceram. Soc.*, **75** [8] 2056-65 (1992)

54 C.A. Calow and A. Moore, "No Hope for Ceramic Whisker or Fibres as Reinforcement of Metal Matrices at High Temperature", *Journal of Materials Science*, 7 543-58 (1972)

55 F.G. Gac, "Synthesis and Characterization of VLS Silicon Carbide Whisker Reinforced Reaction Bonded Silicon Nitride", PhD Thesis, University of Washington, Seattle, Washington 1989

56 J.D. Eshelby, "The Determination of the Elastic Field of an Ellipsoidal Inclusion, and Related Problems", *Proc. R. Soc.*, Lond. **241A** 376-96 (1957)

57 C.H. Hsueh, A.G. Evans, R.M. Cannon, and R.J. Brook, "Viscoelastic Stresses and Sintering Damage in Heterogeneous Powder Compacts", *Acta Metall.*, **34** [5] 927-936 (1986)

58 S. Sundaresan and I.A. Aksay, "Sintering with Rigid Inclusions: Pair Interactions", *J. Am. Ceram. Soc.*, **73** [1] 54-60 (1990)

59 R.K. Bordia and R.Raj, "Sintering of TiO_2-Al_2O_3 Composites: A Model Experimental Investigation ", *J. Am. Ceram. Soc.*, **71** [4] 302-10 (1988)

60 L.C. De Jonghe and M.N. Rahaman, "Sintering of Ceramic Particulate Composites: Effect of Matrix Density", *J. Am. Ceram. Soc.*, **74** [2] 433-36 (1991)

61 R. Zallen, "The Physics of Amorphous Solids", John Wiley & Sons, New York, NY 1983

62 D. Stauffer, "Introduction to Percolation Theory", Taylor & Francis, London, England 1985

63 G.C. Wei and P.F. Becher, "Development of SiC-Whisker Reinforced Ceramics", *J. Am. Ceram. Soc.*, **64** [2] 298-304 (1985)

64 L.C. De Jonghe, M.Y. Chu, and M.N. Rahaman, "Effect of Green Density and Creep During Sintering", *J. Am. Ceram. Soc.*, **74** [3] 514-19 (1991)

65 M. Schwartz, "Handbook of Structural Ceramics", McGraw-Hill, inc., New York, NY 1992

66 P. Boch, "Ceramic Processes: Powders in Suspensions-Slip Casting", *J. Mat. Edu.*, **6** [3] 365-397 (1984)

67 R.G. Horn, "Surface Forces and Their Action in Ceramic Materials", *J. Am. Ceram. Soc.*, **73** [5] 1117-35 (1990)

68 B.J. Kellet and F.F. Lange, "Thermodynamics of Densification: I, Sintering of Simple Particle Arrays, Equilibrium Configurations, Pore Stability, and Shrinkage", *J. Am. Ceram. Soc.*, **72** [5] 725-34 (1989)

69 S.L. Dole, S. Prochazka, R.H. Doremus, "Microstructural Coarsening During Sintering of Boron Carbide", *J. Am. Ceram. Soc.*, **72** [6] 958-66 (1989)

70 S.T. Lin and R.M. German, "Compressive Stress for Large-Pore Removal in Sintering", *J. Am. Ceram. Soc.*, **71** [10] C432-C433 (1988)

71 J. Zhao and M.P. Harmer, "Effect of Pore Distribution on Microstructure Development: I, Matrix Pores", *J. Am. Ceram. Soc.*, **71** [2] 113-20 (1988)

72 R Raj, "Analysis of the Sintering Pressure", *J. Am. Ceram. Soc.*, **70** [9] C210-C211 (1987)

73 S.T. Kwon, D.Y. Kim, T.K. Kang, D.N. Yoon, "Effect of Sintering Temperature on the Densification of Al_2O_3", *J. Am. Ceram. Soc.*, **70** [4] C69-C70 (1987)

74 F.F. Lange and M.M. Hirlinger, "Grain Growth in Two-Phase Ceramics: Al_2O_3 Inclusions in ZrO_2", *J. Am. Ceram. Soc.*, **70** [11] 827-30 (1987)

75 M.Y. Chu, M.N. Rahaman, and L.C. De Jonghe, "Effect of Heating Rate on Sintering and Coarsening", *J. Am. Ceram. Soc.*, **74** [6] 1217-25 (1991)

76 H.L. Hsieh and T.T. Fang, "Effect of Green States on Sintering Behavior and Microstructural Evolution of High-Purity Barium Titanate", *J. Am. Ceram. Soc.*, **73** [6] 1566-73 (1990)

77 L.A. Xue and R.J. Brook, "Promotion of Densification by Grain Growth", *J. Am. Ceram. Soc.*, **72** [2] 341-44 (1989)

78 A.R. West, "Solid State Chemistry and its Applications", John Wiley & Sons, New York, NY 1989

79 W.D. Kingery, H.K. Bowen, and D.R. Uhlmann, "Introduction to Ceramics", 2nd ed., John Wiley & Sons, New York, NY 1976

80 R.M. German, "Liquid Phase Sintering", Plenum Press, New York, NY 1985

81 R.C. Garvie, R.H. Hannink, R.T. Pascoe, "Ceramic Steel?", *Nature*, **258** 703-4 (1975)

82 D.J. Green, R.H.J. Hannink, M.V. Swain, Transformation Toughening of Ceramics, CRC Press, Inc., Boca Raton, FL, 1989

83 A.G. Evans and A.H. Heuer, "Review - Transformation Toughening in Ceramics: Martensitic Transformations in Crack-Tip Stress Fields", *J. Am. Ceram. Soc.*, **63** [5-6] 241-8 (1980)

84 F.F. Lange and K.T. Miller, "Pressure Filtration: Consolidation Kinetics and Mechanics", *Am. Ceram. Soc. Bull.*, **66** [10] 1498-1504 (1987)

85 T.J. Fennelly and J.S. Reed, "Mechanics of Pressure Slip Casting", *J. Am. Ceram. Soc.*, **55** [5] 264-8 (1972)

86 M. Rivier and A.D. Pelton, "A New Slip-Casting Technique for the Laboratory Fabrication of ß-Al_2O_3 and Other Ceramics", *Bull. Am. Ceram. Soc.*, **57** [2] 183-5 (1978)

87 P.A. Smith and R.A. Haber, "Reformulation of an Aqueous Alumina Slip Based on Modification of Particle-Size Distribution and Particle Packing", *J. Am. Ceram. Soc.*, **75** [2] 290-94 (1992)

88 O. Sudre and F.F. Lange, "Effect of Inclusions on Densification: I, Microstructural Development in an Al_2O_3 Matrix Containing a High Volume Fraction of ZrO_2 Inclusions", *J. Am. Ceram. Soc.*, **75** [3] 519-24 (1992)

89 F.F. Lange and M. Metcalf, "Process Related Fracture Origins: II, Agglomerate Motion and Cracklike Internal Surfaces Caused by Differential Sintering", *J. Am. Ceram. Soc.*, **66** [6] 398-406 (1983)

90 J.S. Papanu, R.J. Adler, M.B. Gorensek, M.M. Menon, "Separation of Fine Particle Dispersions Using Periodic Flows in a Spinning Coiled Tube", *AIChE Journal*, **32** [5] 798-808 (1986)

91 F.F. Lange, B.I. Davis, D.O. Raleigh, "Transformation Strengthening of ß"-Al_2O_3 with Tetragonal ZrO_2", *Am. Ceram. Soc.*, **66** [3] C-50-52 (1983)

92 O. Sudre, G. Bao, B. Fan, F.F. Lange, A.G. Evans, "Effect of Inclusions on Densification: II, Numerical Model", *J. Am. Ceram. Soc.*, **75** [3] 519-524 (1992)

93 W. Byckalo, G. Rosenblatt, J. Lam, P.S. Nicholson, "Slip Casting of ß-Al_2O_3 for Alkali Probes in Molten Metals", *Bull. Am. Ceram. Soc.*, **55** [3] 286-8 (1976)